

The Influence of Substrate Structure on Membrane Adhesion

Peter S. Swain^(1,2) and David Andelman⁽²⁾

⁽¹⁾Max-Planck Institut für Kolloid- und Grenzflächenforschung,
14424 Potsdam, Germany

⁽²⁾School of Physics and Astronomy,
Raymond and Beverly Sackler Faculty of Exact Sciences,
Tel Aviv University, Ramat Aviv 69978, Tel Aviv, Israel

Abstract

We consider a membrane both weakly and strongly adhering to a geometrically structured substrate. The interaction potential is assumed to be local, via the Deryagin approximation, and harmonic. Consequently, we can analytically describe a variety of different geometries: as well as randomly rough self-affine surfaces, smooth substrates interrupted by an isolated cylindrical pit, a single elongated trench or a periodic array of trenches are investigated. We present more general expressions for the adhesion energy and membrane configuration in Fourier space and find that, compared to planar surfaces, the adhesion energy decreases. We also highlight the possibility of overshoots occurring in the membrane profile and look at its degree of penetration into surface indentations.

1 Introduction

The statistical mechanics of membranes is an important branch of soft-condensed matter physics, not least because of its application to biological systems. Examples of membranes that can be studied experimentally include liposomes or vesicles, microemulsions, lamellar liquid crystals, as well as biological cells, such as red blood cells [1]. Of great importance is a detailed understanding of the adhesion between two membranes or between a membrane and a substrate. This occurs ubiquitously in nature, with vesicle adhesion playing a dominant role in endo- and exocytosis [2], that is the communication of a cell with its immediate environment. Efficient drug delivery is dependent on the adhesion between a liposome and the plasma membrane of the target site [3] while adhesion phenomena are also indispensable to biotechnology with, for example, biosensors being based on the binding of membranes to substrates.

In this paper we choose to concentrate on the latter, that is the adhesion between a membrane and a solid substrate, in order to provide theoretical support for recent experiments aimed at creating new biotechnology. All of this research has involved the study of adhesion on materials which are not flat and chemically homogeneous but that have a deliberate chemical or geometrical patterning. As far as we are aware, there has been no theoretical work describing membrane adhesion on such structured surfaces. Previous studies have looked at vesicle adhesion on simple, planar, chemically homogeneous substrates [4, 5] and we hope now to redress this imbalance.

First of all, we distinguish between weakly and strongly adhering vesicles or membranes. Weakly adhering giant vesicles have been studied using reflection interference contrast microscopy [6] and have been found to lie at distances between 300 Å and 400 Å from a planar substrate. Here, Van der Waals attractions to the substrate are mainly counterbalanced by a repulsive entropic Helfrich force. Strongly adhering or supported membranes [7], however, sandwich a water or polymer film between them and the substrate and typically have a much smaller separation lying at distances between 10 Å and 40 Å. Hydration forces are now the dominant repulsive interaction.

Supported membranes provide perhaps the most potential for biotechnological applications. They can be formed by the spreading of a bilayer over a substrate, vesicle fusion taking place at a substrate or by lipid monolayer transfer using a Langmuir-Blodgett technique [7]. These membranes are useful as they enable bio-functionalization of inorganic solids and provide a means to immobilize proteins, e.g. lipid coupled antigens and antibodies, with a well defined orientation and in non-denaturing conditions [8]. This then offers a suitable environment to investigate protein-membrane coupling and protein-protein recognition processes. They also can be used to design phantom cells which allow study of the interplay between specific (lock and key) and universal forces during cell adhesion [7].

However, we wish to highlight the ability of supported membranes to act as biosensors. They can provide ultra-thin, highly electrically resistant layers on top

of a conducting substrate. If protein receptors are incorporated into these layers then electrical or optical detection of ligand binding to the receptors creates a biosensor. Alternatively, protein ion channels can be embedded in the membrane in which case their effect on its permeability endows the membrane with sensor-like properties.

Proteins included in the membrane often have a dimension greater than its thickness (which is approximately 40\AA) and so can lift the membrane off the substrate. This is undesirable and can be prevented by creating water pockets on the surface of the substrate which then act as protein “docking” sites. Therefore, one is naturally led to consider membrane adhesion on geometrically structured substrates which have been indented in some way. This structure can be made by a variety of methods, for example, chemical etching of silicon wafers can lead, due to their particular crystal structure, to long “V”-shaped channels [9]. Alternatively, one can use micelles made from diblock copolymers to coat any semiconductor wafer. If this is ion sputtered, then loading of the micelles before hand with an inorganic compound can provide large etching contrasts. Using this technique one can pattern a planar substrate with pits or islands on a nanometer scale [10].

Motivated by such experiments, we discuss here a straightforward theoretical approach which allows the adhesion energy of a bound membrane to be calculated for a variety of different geometrical configurations of the substrate. The techniques used have been strongly influenced by recent work in wetting phenomena. There is now quite a substantial literature covering the effect of geometrical and chemical substrate structure on wetting films. A general form of Young’s equation has been derived [11, 12], the influence of disorder [13] and corrugation [14] of the substrate on wetting transitions determined and the effect of chemical patterning [15] on the shapes of adhering droplets studied. However, we use as the inspiration for our approach, a systematic description of the configuration of wetting films on non-planar surfaces [16, 17, 18] in which the full non-local form of the Van der Waals interaction can be accounted for.

There are also many interesting applications involving the adhesion of membranes on chemically structured substrates. However, we will not discuss this further here but return to it again in an accompanying publication [19].

To start, we describe the various molecular interactions included in our model and differentiate between strong and weak adhesion. In Sec. 3, we consider simple, planar surfaces, which serve as basis for nearly all the following work. The most profitable analytic approach, the Deryagin approximation, is detailed in Sec. 4. We consider (separately) a corrugated substrate (Sec. 4.1) and one broken by a single (long) trench (Sec. 4.3), a pit (Sec. 4.4) and a periodic array of trenches (Sec. 4.5). We calculate the equilibrium membrane profile and the adhesion energy. The variation of this energy with respect to the parameters characterizing the geometric structure is emphasized. In Sec. 4.6, the adhesion energy for randomly rough or self-affine surfaces is given for two particular cases. Finally, we conclude with a short discussion.

2 The Free Energy

To begin, we consider a membrane with an elastic modulus κ and tension σ interacting with a rough surface. For a free, almost flat membrane, which is infinite in extent, the bending energy can be described by an effective free energy functional [20]

$$\int ds_1 ds_2 \sqrt{g} \left[\sigma + \frac{1}{2} \kappa (2H)^2 \right] \quad (2.1)$$

where (s_1, s_2) are coordinates in the membrane surface, g is the determinant of the metric, $H = (c_1 + c_2)/2$ the mean curvature, and c_1 and c_2 the two principal curvatures. As the Gaussian curvature is a total divergence, the Gauss-Bonnet theorem implies that it can be ignored for a membrane with fixed topology and we proceed to do just this here. Working in the Monge representation, let $\boldsymbol{\rho} = (x, y)$ be a two dimensional planar vector and the heights of the surface and membrane above some reference $\boldsymbol{\rho}$ -plane be $z_s(\boldsymbol{\rho})$ and $h(\boldsymbol{\rho})$, respectively. The geometry and notation used is shown in Fig. 1.

For an experimental system, in which giant vesicles (rather than the infinite membrane considered here) are involved, the tension usually arises due to the conservation of the vesicle total surface area. However, an additional contribution develops, for a weakly adhering vesicle, as the lipids making up the membrane try and move from areas far from the substrate into the more energetically favorable region near the surface. However, for our case of an infinite membrane none of these intricacies arise and we can consider the tension as an external parameter.

If the membrane thickness is δ , the interaction between the surface and the membrane can be accounted for by a potential $V(h, \delta; z_s)$ and total membrane free energy is given as

$$\mathcal{F}[h] = \int d\boldsymbol{\rho} \left\{ \sqrt{1 + (\nabla h)^2} \left[\sigma + \frac{\kappa}{2} \left(\nabla \cdot \frac{\nabla h}{\sqrt{1 + (\nabla h)^2}} \right)^2 \right] + V(h, \delta; z_s) \right\} \quad (2.2)$$

where we have used the Monge representation.

The interaction can be broken down into several components [21, 22]. We will always include an external pressure, a Van der Waals attraction and a repulsive force, whose nature will be different for strong and weak adhesion. In principle, other possible interactions, for example electrostatic forces, can be added for more refined calculations. The total potential, used in (2.2), is then

$$V(h, \delta; z_s) = p \cdot (h - z_s) + V_{\text{vdw}}(h, \delta; z_s) + V_{\text{rep}}(h; z_s) \quad (2.3)$$

A different dependence on the surface height has been emphasized as, in general, the interaction potential is a *functional* of z_s . Note that in (2.2), the potential V is integrated over the *projected area*, $A_0 = \int d\boldsymbol{\rho}$, only because all non-local effects of the solid roughness and membrane fluctuations are, in principle, incorporated into the potential itself.

The existence of an external pressure p in (2.3) implies that there is a difference in pressure across the membrane. Recalling that the membrane is infinite in its lateral extent, the pressure couples linearly to the membrane height and could arise, for example, from the existence of macromolecules on one side of the membrane only. An additional contribution arises due to the finite membrane thickness but as we assume that this is fixed throughout the membrane, it is just a constant which we neglect.

The Van der Waals attraction that the membrane feels towards the solid surface is given by

$$V_{\text{vdw}}(h, \delta; z_s) = -[W(h; z_s) - W(h + \delta; z_s)] \quad (2.4)$$

where $W(h; z_s)$ is an interfacial-like Van der Waals potential. Equation (2.4) arises due to the bilayer nature of the membrane and can be understood as a supposition of two wetting layers. One of these has height $h + \delta$ while the other is of height h and has a Hamaker constant of opposite sign. For a wetting fluid film of thickness $h(\boldsymbol{\rho})$ resting on a solid substrate, with a rough surface configuration given by $z = z_s(\boldsymbol{\rho})$, $W(h; z_s)$ satisfies [16]

$$W(h; z_s) = \int_{h(\boldsymbol{\rho})}^{\infty} dz \int d\boldsymbol{\rho}' \int_{-\infty}^{z_s(\boldsymbol{\rho}+\boldsymbol{\rho}')} dz' w(\boldsymbol{\rho}', z - z') \quad (2.5)$$

with a kernel interaction

$$w(\mathbf{r}) = \frac{A}{\pi^2} \left(\frac{1}{r}\right)^{2m+2} \quad (2.6)$$

Following convention, we have denoted the Hamaker constant by A and will usually set the integer $m = 2$ to model non-retarded Van der Waals interactions. Equation (2.5) comes from the sum over all possible pair interactions between the molecules making up two half spaces which are each capped by either the surface $z = h(\boldsymbol{\rho})$ or $z = z_s(\boldsymbol{\rho})$.

Notice that (2.5) is a function of $h(\boldsymbol{\rho})$ but a functional of $z_s(\boldsymbol{\rho})$. For a flat membrane on top of a smooth and planar solid surface, which will be discussed in the following section, this functional dependence on $z_s(\boldsymbol{\rho})$ can be ignored and then (for $m = 2$)

$$W(h, z_s) = \frac{A}{12\pi} \cdot \frac{1}{(h - z_s)^2} \quad (2.7)$$

This is the standard result for the Van der Waals potential between two semi-infinite bodies with planar surfaces held a distance $h - z_s$ apart [22].

To counterbalance this attractive force, a repulsive interaction is included and, as before, we define two different possible scenarios; the weak and strong adhesion regimes:

2.1 Weakly adhering membranes

In this case we consider a repulsive force which is entropic in origin. This arises due to the surface cutting off the region that can be sampled by the membrane

as it undergoes thermal fluctuations. A renormalization group description is the only general approach that can be used to describe such effects but, providing fluctuations do not become critical, a simple supposition ansatz can suffice [21]. In this, so-called weak fluctuation regime [23], an entropically based term is added to the membrane potential. Such a term was first described by Helfrich [24] for a membrane (with zero tension) in a stack of membranes and can be thought of as an ideal “gas” pressure. The presence of another membrane above and below introduces a new lengthscale describing the maximum wavelength at which any membrane within the stack can fluctuate without being strongly suppressed by its neighbors. Fluctuations with wavelengths below this lengthscale are essentially unhampered and so one can think of an ideal gas of uncorrelated membrane humps characterized by a single size. The pressure that this gas exerts is simply the Helfrich repulsion.

When a membrane is under tension, the extent to which it can fluctuate is much reduced. Therefore, in some sense, the membrane “feels” the presence of a surface or another membrane less and there is a corresponding decrease in entropic repulsion. This effect was looked at by Helfrich and Servuss [25], who, within a mean-field theory, found that the entropic repulsion, between two membranes, decayed exponentially in h^2 in the tension-dominated regime. Such a result has also been confirmed by Evans [26] via a self-consistent mean-field method. However, by using a functional renormalization group approach [21] to include thermal fluctuations, it has been argued that this decay, while remaining exponential, should be so in h only. This has been verified by Monte-Carlo simulation [27]. Analytical forms of the entropic repulsion are only available for the tension and rigidity dominated regimes but ideally one would like to have a function which tends to these two expressions in the appropriate limits. While this function has been found numerically [27], there does not yet exist a complete analytical expression for it. However, a simple argument by Seifert [5] gives a form of the entropic interaction which takes the correct limit for $\sigma \rightarrow 0$ or $h \rightarrow 0$ and has the dominant exponential decay in h also present in the tension regime. We choose, for simplicity, to adopt this form which is given by

$$V_{\text{fluc}}(h) = \frac{6T^2}{(2\pi)^2\kappa} \left(\frac{\Omega}{\sinh \Omega h} \right)^2 \quad (2.8)$$

where

$$\Omega = \left(\frac{\pi\sigma}{2T} \right)^{\frac{1}{2}} \quad (2.9)$$

We denote the temperature by T and have set here and hereafter the Boltzmann constant k_B to unity. The prefactor of (2.8) has been chosen to be consistent with the renormalization group description [21] as $h \rightarrow \infty$ but we note that the exact value has no special importance in the model presented here. In the limit of zero tension ($\sigma/ka \sim \sigma/T \rightarrow 0$), (2.8) tends to the well known result $3T^2/(2\pi^2\kappa h^2)$. For large Ωh , the potential decays exponentially as $\exp(-2\Omega h)$. In this limit, which can correspond to large σ , the membrane should take on more interfacial-like

behavior and, indeed, the entropic repulsion for an interface in three dimensions is also expected to decay exponentially with height [23].

As δ is constant we can ignore its influence on the fluctuation interaction; it is only the lower lipid leaflet which defines the volume between the membrane and the substrate and so determines V_{fluc} .

Equation (2.8) was initially assumed only to be valid for a membrane fluctuating near a flat surface. However, a number of different methods have shown that the Helfrich term can also be used for a rough substrate if h is replaced by the local height of the membrane. This approach has been adopted by several authors considering spatially inhomogeneous scenarios [28, 29, 30] and agrees with scaling arguments based on exact solutions [31]. For temperatures nearing the unbinding temperature, where the thermal fluctuations of the membrane go critical [32], the validity of (2.8) can be questioned and so throughout this paper we will only consider temperature regimes far from the unbinding transition. Consequently, for a rough surface, we choose a fluctuation repulsion satisfying $V_{\text{fluc}}(h; z_s) = V_{\text{fluc}}(h - z_s)$, with $V_{\text{fluc}}(h)$ given by (2.8).

2.2 Strongly adhering membranes

As the membrane now lies much closer to the substrate (a typical distance can be 30\AA as compared with 340\AA for the weakly adhering case), the repulsive interaction becomes dominated by hydration forces. While their exact origin is not entirely understood, see [22], experimentally they decay exponentially [33] and have an Angstrom range,

$$V_{\text{hyd}}(h) = b\sigma e^{-\alpha h} \quad (2.10)$$

where b is a dimensionless number and α an inverse length, typically $\alpha^{-1} \simeq 2\text{--}3\text{\AA}$. For a rough substrate we again assume that we can replace h by the relative height and so use the local expression for the interaction potential, $V_{\text{hyd}}(h - z_s)$, in the free energy. Such an assumption seems reasonable due to the very short-range nature of the interaction in (2.10).

2.3 The adhesion energy

To summarize, the total free energy consists of

$$\mathcal{F}[h] = \int d\rho \left\{ \sqrt{g} \left[\sigma + \frac{1}{2} \kappa (2H)^2 \right] + p \cdot (h - z_s) + V_{\text{vdw}}(h, \delta; z_s) + V_{\text{rep}}(h - z_s) \right\} \quad (2.11)$$

that is, a bending energy, made up of tension (coupled to the membrane area) and rigidity (coupled to its total mean curvature squared, H^2) terms, and an interaction potential V given by (2.3). The latter contains a contribution from an external pressure, the full non-local Van der Waals interaction and a local repulsion, V_{rep} , which we consider either as a fluctuation, see (2.8), or a hydration interaction as in (2.10).

One of the most relevant quantities in experiments is the membrane adhesion energy. Within our general mean-field approach, the optimal height of the membrane is that which minimizes (2.11). The value of the free energy of the system when the membrane takes up this optimum configuration, \mathcal{F}_{\min} , leads to a natural definition of the adhesion energy per unit area

$$U \equiv - \left(\frac{\mathcal{F}_{\min}}{A_0} - \sigma \right) \quad (2.12)$$

Here, A_0 is the total area of the *projected* reference $\boldsymbol{\rho}$ -plane, $A_0 = \int d\boldsymbol{\rho}$.

Notice that in the above equation a tension dependent term is subtracted from the definition of the adhesion energy. Doing so conveniently shifts the origin in such a way that the adhesion energy for a completely flat membrane has no tension dependent contribution. This agrees with one's intuitive picture and is necessary as the membrane tension couples to the entire membrane area and not just to any excess area arising from a non-planar configuration. Consequently, for a membrane adhering to a flat wall and being itself flat, $h(\boldsymbol{\rho}) = h_0$ for some constant h_0 , the adhesion energy is simply given as the negative of the interaction potential experienced by the membrane. For example, from (2.11), [see also (2.2)],

$$\mathcal{F}_{\min} = A_0 [\sigma + V(h_0, \delta; 0)] \quad (2.13)$$

and so (2.12) implies that

$$U = -V(h_0, \delta; 0) \quad (2.14)$$

and the tension contribution vanishes. Hence, U is positive for all sufficiently attractive potentials, V .

2.4 Rescaling of lengths and interactions

Before we proceed and calculate the adhesion energy U for different types of corrugated and rough surfaces, it proves profitable to extract two natural lengthscales present in the problem.

The first of these is provided by the ratio between the Hamaker constant, A , appearing in the Van der Waals potential (2.5), and the tension σ [34],

$$a = \left(\frac{A}{2\pi\sigma} \right)^{\frac{1}{2}} \quad (2.15)$$

while the second describes the crossover between the tension and the rigidity dominated regimes

$$\xi = \sqrt{\frac{\kappa}{\sigma}} \quad (2.16)$$

Using these definitions (2.2) becomes

$$\frac{1}{\sigma} \mathcal{F}[h] = \int d\boldsymbol{\rho} \left\{ \sqrt{1 + (\nabla h)^2} \left[1 + \frac{1}{2} \xi^2 \left(\nabla \cdot \frac{\nabla h}{\sqrt{1 + (\nabla h)^2}} \right)^2 \right] + \frac{1}{\sigma} V(h, \delta; z_s) \right\} \quad (2.17)$$

Equation (2.5) gives

$$\frac{1}{\sigma}W(h; z_s) = \frac{2a^2}{\pi} \int_{h(\boldsymbol{\rho})}^{\infty} dz \int d\boldsymbol{\rho}' \int_{-\infty}^{z_s(\boldsymbol{\rho}+\boldsymbol{\rho}')} dz' [\boldsymbol{\rho}'^2 + (z - z')^2]^{-(m+1)} \quad (2.18)$$

while the fluctuation and hydration interactions can be written, respectively, as

$$\frac{1}{\sigma}V_{\text{fluc}}(h) = \frac{3T}{4\pi\kappa} \sinh^{-2}(\Omega h) \quad (2.19)$$

and

$$\frac{1}{\sigma}V_{\text{hyd}}(h) = b e^{-\alpha h} \quad (2.20)$$

where $\Omega = (\pi\sigma/2T)^{1/2}$ was defined earlier.

In the next sections (2.17) will be minimized and the adhesion energy U will be calculated for various corrugated and rough surfaces. However, first we discuss the case of a simple, flat surface.

3 A planar surface: choice of physical parameters

For a planar and homogeneous solid surface, mean-field theory predicts that the membrane also adopts a flat configuration,

$$h(\boldsymbol{\rho}) = h_0 \quad (3.1)$$

where we use the subscript zero to denote all planar quantities. Here, we set $z_s(\boldsymbol{\rho}) = 0$ in order to ensure a zero average surface height. The Van der Waals term (for $m = 2$) also simplifies considerably

$$\frac{1}{\sigma}V_{\text{vdw}}(h, \delta; 0) = -\frac{a^2}{6} \left(\frac{1}{h^2} - \frac{1}{(h + \delta)^2} \right) \quad (3.2)$$

while the repulsion satisfies (2.19) and (2.20) for weak and strong adhesion, respectively.

The membrane height h_0 obeys $V' = \frac{\partial V}{\partial h} = 0$ (balance of forces), that is

$$V'(h_0) = p + \frac{\sigma a^2}{3} \left(\frac{1}{h_0^3} - \frac{1}{(h_0 + \delta)^3} \right) + V'_{\text{rep}}(h_0) = 0 \quad (3.3)$$

with an adhesion energy, (2.12), of

$$\begin{aligned} -\frac{U_0}{\sigma} &\equiv \frac{V_0(h_0, \delta)}{\sigma} \\ &= \begin{cases} \frac{p}{\sigma} h_0 - \frac{a^2}{6} \left[\frac{1}{h_0^2} - \frac{1}{(h_0 + \delta)^2} \right] + \frac{3T}{4\pi\kappa} \sinh^{-2}(\Omega h_0) & \text{weak adhesion} \\ \frac{p}{\sigma} h_0 - \frac{a^2}{6} \left[\frac{1}{h_0^2} - \frac{1}{(h_0 + \delta)^2} \right] + b e^{-\alpha h_0} & \text{strong adhesion} \end{cases} \quad (3.4) \end{aligned}$$

where $V_0(h, \delta) \equiv V(h, \delta; 0)$. Equation (3.4) is useful as it serves as the starting point to which all our perturbation theories provide corrections.

At this point in order to facilitate comparison with experimental systems we discuss the numerical values of our model parameters. A particular example is detailed in Table 1, where $T = 4.1 \times 10^{-21}$ J at room temperature and k_B was set to unity. For simplicity, the external pressure is set equal to zero throughout

$$p = 0 \tag{3.5}$$

Let us discuss now the choice of parameters for weak and strong adhering membranes, separately:

(i) For weak adhesion, an effective value of the Hamaker constant is used, $A = 8.67 \times 10^{-22}$ J $\simeq 0.21 T$. This value is quite small in order to approximately model the screening effect of ions in the solution surrounding the membrane [22]. Setting $\sigma = 1.7 \times 10^{-5}$ Jm $^{-2}$, the rescaling length, $a \simeq 28.5$ Å, and h_0 is calculated to be $h_0 \simeq 11.85a \simeq 338$ Å, in agreement with experiment [6]. Such a value is reassuring as the expression, (3.2) for the Van der Waals interaction, is only valid for $h < 500$ Å before retardation effects begin to become important [32]. From Fig. 2, one can see that $V_0(h_0, \delta) \simeq -1.1 \times 10^{-4}\sigma$ and so the adhesion energy

$$\begin{aligned} U_0 &\equiv -V_0(h_0, \delta) \\ &\simeq 1.1 \times 10^{-4}\sigma = 1.87 \times 10^{-9} \text{ Jm}^{-2} \end{aligned} \tag{3.6}$$

which is positive as expected.

(ii) If we now turn to strong adhesion, ion effects can be ignored and we use a larger value of the Hamaker constant, $A = 2.6 \times 10^{-21}$ Jm $^{-2} \simeq 0.63 T$ [6]. This implies that $a \simeq 49.3$ Å and $h_0 \simeq 0.61a \simeq 30$ Å in agreement with measured values using specular reflection of neutrons [35]. The various parameters specifying the hydration force, see (2.10), are

$$b = (0.93 \text{ Jm}^{-2})/\sigma \simeq 5.47 \times 10^4 \quad ; \quad \alpha^{-1} = 2.2 \text{ Å} \tag{3.7}$$

which are in accordance with those measured in [33]. This time, see Fig. 2, $V_0(h_0, \delta) \simeq -0.298\sigma$ and so

$$U_0 \simeq 0.298\sigma = 5.07 \times 10^{-6} \text{ Jm}^{-2} \tag{3.8}$$

which is significantly greater than (3.6).

Throughout the paper, we will keep to the particular values of the membrane and external parameters specified here and in Table 1. It is sometimes convenient to express lengths in terms of the length a and energies (per unit area) in terms of the tension σ , which is arbitrarily taken to have the same numerical value for weak and strong adhering membranes. We should say though that our model can offer only qualitative, or at best semi-quantitative comparison with experiment.

4 The Deryagin approximation

One of the most useful approaches, which provides good opportunity for analytic progress, is the Deryagin approximation [36]. First of all, the full non-local Van der Waals potential, (2.4) and (2.5), is replaced by a planar potential which is simply a function of the local relative height coordinate. Since the pressure term is always local and V_{rep} already has this form, the total potential is written as

$$\begin{aligned} V(h, \delta; z_s) &\simeq V_0(h - z_s, \delta) \\ &= p \cdot (h - z_s) + V_{\text{vdw}}(h - z_s, \delta; 0) + V_{\text{rep}}(h - z_s) \end{aligned} \quad (4.1)$$

where $V_0(h, \delta) = V(h, \delta; 0)$ as before. Notice that the above expression corresponds to replacing $z_s(\boldsymbol{\rho} + \boldsymbol{\rho}')$ in (2.5) with $z_s(\boldsymbol{\rho})$, i.e. removing the functional dependence of the potential on z_s . The resulting free energy is then expanded to second-order in $h - h_0$ and z_s . Since the equilibrium position of the membrane is given by setting the variation to zero, the first-order term in h and z_s vanishes, yielding

$$\frac{1}{\sigma} \mathcal{F}[h] \simeq \int d\boldsymbol{\rho} \left\{ 1 + \frac{1}{2} (\nabla h)^2 + \frac{1}{2} \xi^2 (\nabla^2 h)^2 + \frac{1}{\sigma} V_0(h_0, \delta) + \frac{v}{2\sigma} (h - h_0 - z_s)^2 \right\} \quad (4.2)$$

with

$$\begin{aligned} v &= \left. \frac{\partial^2}{\partial h^2} V(h, \delta; 0) \right|_{h=h_0} \\ &= -a^2 \sigma \left[\frac{1}{h_0^4} - \frac{1}{(h_0 + \delta)^4} \right] + V''_{\text{rep}}(h_0) \end{aligned} \quad (4.3)$$

and

$$V''_{\text{rep}}(h_0) = \begin{cases} \frac{3\sigma}{4\xi^2} [2 + \cosh(2\Omega h_0)] \sinh^{-4}(\Omega h_0) & \text{weak adhesion} \\ \sigma \alpha^2 b e^{-\alpha h_0} & \text{strong adhesion} \end{cases} \quad (4.4)$$

Writing $\delta h(\boldsymbol{\rho}) = h(\boldsymbol{\rho}) - h_0$, the Euler-Lagrange equation, giving the value of δh which minimizes (4.2), is relatively straightforward

$$\left(\kappa \nabla^4 - \sigma \nabla^2 + v \right) \delta h(\boldsymbol{\rho}) = v z_s(\boldsymbol{\rho}) \quad (4.5)$$

To solve (4.5), it is convenient to convert to Fourier space. Defining for any function $f(\boldsymbol{\rho})$

$$\tilde{f}(\mathbf{q}) = \int d\boldsymbol{\rho} f(\boldsymbol{\rho}) e^{-i\mathbf{q} \cdot \boldsymbol{\rho}} \quad (4.6)$$

we find

$$\tilde{\delta h}(\mathbf{q}) = \frac{\tilde{z}_s(\mathbf{q})}{1 + q^2 \xi_\sigma^2 + q^4 \xi_\kappa^4} \quad (4.7)$$

with the correlation lengths, having the usual definitions [21]

$$\xi_\sigma^2 = \sigma/v \quad ; \quad \xi_\kappa^4 = \kappa/v \quad (4.8)$$

For small $q\xi_\sigma$, (4.7) implies that the membrane follows the rough surface. However, as $q\xi_\sigma$ increases, both the tension and the rigidity act to dampen this effect.

Using (2.12, 4.2) and (4.7), one can write down the adhesion energy

$$\begin{aligned}
\frac{U}{\sigma} - 1 + \frac{1}{A_0} \int d\rho \left\{ 1 + \frac{V_0(h_0, \delta)}{\sigma} \right\} \\
= -\frac{v}{A_0\sigma} \int \frac{d\mathbf{q}}{2(2\pi)^2} \left\{ (1 + q^2\xi_\sigma^2 + q^4\xi_\kappa^4) |\delta\tilde{h}(\mathbf{q})|^2 + |\tilde{z}_s(\mathbf{q})|^2 - 2\delta\tilde{h}(\mathbf{q})\tilde{z}_s(-\mathbf{q}) \right\} \\
= -\frac{v}{A_0\sigma} \int \frac{d\mathbf{q}}{2(2\pi)^2} \left\{ \frac{q^2\xi_\sigma^2 + q^4\xi_\kappa^4}{1 + q^2\xi_\sigma^2 + q^4\xi_\kappa^4} \right\} |\tilde{z}_s(\mathbf{q})|^2
\end{aligned} \tag{4.9}$$

By defining the excess in the adhesion energy to be with respect to the planar case [recall that $U_0 = -V_0(h_0, \delta)$]

$$\begin{aligned}
\Delta U &\equiv U - U_0 \\
&= U + V_0(h_0, \delta)
\end{aligned} \tag{4.10}$$

we obtain

$$\frac{\Delta U}{\sigma} = -\frac{1}{A_0} \int \frac{d\mathbf{q}}{2(2\pi\xi_\sigma)^2} \left\{ \frac{q^2\xi_\sigma^2 + q^4\xi_\kappa^2}{1 + q^2\xi_\sigma^2 + q^4\xi_\kappa^4} \right\} |\tilde{z}_s(\mathbf{q})|^2 \tag{4.11}$$

which is only strictly valid up to $O(q^4)$ as higher order terms in q have not been included in our starting equation.

Equation (4.11) has buried within it several assumptions which we would now like to make more explicit. It is important to realize that (4.7) is not necessarily the general solution to (4.5) but just a particular solution. The general solution itself can be found by adding (4.7) to the homogeneous solution, that is the solution of (4.5) when z_s is set to zero. This then contains the four constants of integration required to satisfy any boundary conditions. Therefore, (4.11) is only correct when the homogeneous solution of (4.5) is identically zero, which is true, for example, at a sinusoidally corrugated substrate (see Sec. 4.1). Otherwise, while (4.11) is certainly included in U , it is not the whole picture and in this case it may well be better to work entirely in real space.

For the particular experimental system specified in Sec. 3, one can calculate the various correlation lengths. These have been included in Table 1 for completeness.

The approximations used in this section have, as their basis, essentially a perturbation theory (assuming $h - h_0 - z_s$ is small) around the planar value of the adhesion energy, U_0 . Generally, one can only believe such an approach if the correction term, ΔU , is much smaller than the result it is trying to improve upon. Consequently, our findings are strictly only valid when

$$\left| \frac{\Delta U}{U_0} \right| \ll 1 \tag{4.12}$$

which in fact limits the roughness of the substrates we can consider.

4.1 Sinusoidally corrugated surface

The simplest case to look at is a sinusoidally corrugated surface

$$z_s(\boldsymbol{\rho}) = c \sin(qx) \quad (4.13)$$

with an amplitude c and period $2\pi/q$. Solving (4.5), one can show that

$$\delta h(\boldsymbol{\rho}) = \frac{c \sin(qx)}{1 + q^2 \xi_\sigma^2 + q^4 \xi_\kappa^4} \quad (4.14)$$

Similarly, ΔU in (4.11) is

$$\frac{\Delta U}{\sigma} = -\frac{c^2}{4\xi_\sigma^2} \left(\frac{q^2 \xi_\sigma^2 + q^4 \xi_\kappa^4}{1 + q^2 \xi_\sigma^2 + q^4 \xi_\kappa^4} \right) \quad (4.15)$$

which is valid for small cq .

In Fig. 3, U/U_0 (using the parameters of Table 1) is plotted as a function of the rescaled wavenumber aq for both weak and strong adhesion. From (4.14), the average height of the membrane is unchanged from the planar result h_0 . However, as q increases and the surface becomes corrugated with shorter wavelengths, the adhesion energy decreases (relative to the planar case) due to the extra bending energy cost as the membrane tries to follow these surface configurations. For large q , U flattens out; any point on the membrane is almost equidistant from a crest or trough on the substrate surface and so there is little energetic benefit in mimicking them. From (4.15), we have, in the limit $q \gg \max(\xi_\sigma^{-1}, \xi_\kappa^{-1})$ [37],

$$\Delta U \simeq -\frac{c^2 \sigma}{4\xi_\sigma^2} \quad (4.16)$$

which is in accordance with $U/U_0 \simeq 0.54$ and $U/U_0 \simeq 0.51$, see Fig. 3, for weak and strong adhesion, respectively. For small $q \ll \min(\xi_\sigma^{-1}, \xi_\kappa^{-1})$, the membrane can always follow these long wavelength perturbations,

$$\Delta U \simeq -\frac{\sigma c^2 q^2}{4} \quad (4.17)$$

and U remains q dependent.

It is worth pointing out the very different x -axis scales and choices of c in Fig. 3. For weak adhesion $c = 5a$, that is $c \simeq 143 \text{ \AA}$, the adhesion energy “bottoms out” for $q \simeq 0.03/a$. For strong adhesion c is much smaller, $c \simeq 8 \text{ \AA}$ and much larger values of q are needed before the structure of the substrate is effectively smeared away. The values of c in both cases were chosen to ensure that (4.12) remains valid and one can see that U/U_0 is never much smaller than 0.5. Our perturbation theory seems to work for amplitudes, c , which do not grow significantly bigger than around one third of the height taken by the membrane above a planar substrate, i.e. $h_0/3$.

By noting that $\xi_\kappa^2 = \xi\xi_\sigma$, (4.15) can be written as

$$\frac{\Delta U}{\sigma} = -\frac{c^2}{4} \left(\frac{q^2}{\frac{1}{1+q^2\xi^2} + q^2\xi_\sigma^2} \right) \quad (4.18)$$

and so one can also look at the effect of the elastic modulus κ on the adhesion energy by plotting U/U_0 against the crossover length ξ/a while keeping ξ_σ constant, see Fig. 4. As ξ increases, κ becomes greater than the strength of the Van der Waals interaction, the Hamaker constant, A . This increased bending energy (coupled with the fact that the membrane average position is fixed at h_0) leads to a raise in magnitude of ΔU and so the adhesion energy decreases relative to U_0 .

4.2 The profile equation for piecewise constant surfaces

In some cases, and in particular if z_s is piece-wise continuous, it is more convenient to work directly in real space (as opposed to Fourier space). The task is then to solve (4.5) and use (4.2) to find U . Given a piecewise constant surface, (4.5) becomes

$$\left(\kappa \nabla^4 - \sigma \nabla^2 + v \right) \left(\delta h(\boldsymbol{\rho}) - z_s \right) = 0 \quad (4.19)$$

for a constant z_s (but which changes value discontinuously for different ranges of $\boldsymbol{\rho}$).

The operator in (4.19) can be factorized

$$\kappa \nabla^4 - \sigma \nabla^2 + v = \kappa \left(\nabla^2 - \eta_+^2 \right) \left(\nabla^2 - \eta_-^2 \right) \quad (4.20)$$

where η_\pm are complex in general and satisfy

$$\eta_\pm = \xi^{-1} \left[\frac{1 \pm \sqrt{1 - 4\chi^4}}{2} \right]^{\frac{1}{2}} \quad (4.21)$$

with

$$\chi = \left(\kappa v / \sigma^2 \right)^{\frac{1}{4}} = \frac{\xi}{\xi_\kappa} \quad (4.22)$$

a dimensionless ratio of lengths. For our chosen set of parameters (Table 1), $\chi \simeq 0.302$ and $\chi \simeq 9.44$ for weak and strong adhesion, respectively.

Therefore, to solve (4.19) which is a 4th order differential equation we can consider, equivalently, two coupled 2nd order differential equations

$$\left(\nabla^2 - \eta_-^2 \right) \left(\delta h(\boldsymbol{\rho}) - z_s \right) = u_0(\boldsymbol{\rho}) \quad (4.23)$$

$$\left(\nabla^2 - \eta_+^2 \right) u_0(\boldsymbol{\rho}) = 0 \quad (4.24)$$

for the function $\delta h(\boldsymbol{\rho})$ and a second function $u_0(\boldsymbol{\rho})$. However, because of the underlying linearity of the 2nd order differential equations, the general solution is simply

$$\delta h(\boldsymbol{\rho}) = c_0 u_0(\boldsymbol{\rho}) + c_1 u_1(\boldsymbol{\rho}) + z_s \quad (4.25)$$

for constant c_0 , c_1 and z_s , and where $u_1(\boldsymbol{\rho})$ satisfies

$$(\nabla^2 - \eta_-^2)u_1(\boldsymbol{\rho}) = 0 \quad (4.26)$$

Thus, we have reduced the 4th order differential equation to two familiar 2nd order Helmholtz equations. This approach is most useful for systems with cylindrical or spherical symmetry. We note that for those with one-dimensional symmetry, $z_s(\boldsymbol{\rho}) = z_s(x)$, it is straightforward to solve the 4th order differential equation (4.19) directly. The general solution is (for constant c_0, c_1, c_2 and c_3)

$$\delta h(x) = c_0 e^{\eta_+ x} + c_1 e^{-\eta_+ x} + c_2 e^{\eta_- x} + c_3 e^{-\eta_- x} + z_s \quad (4.27)$$

which we will use in the following sections.

4.3 An isolated trench

We next consider a single, infinitely long trench parallel to the y axis and of width d and depth λd . The height profile of the surface takes either of two fixed values: $-\lambda d$ for $|x| < d/2$, and zero otherwise (see Fig. 5). This can be also written as

$$z_s(\boldsymbol{\rho}) = z_s(x) = -\lambda d \{ \theta(x + d/2) - \theta(x - d/2) \} \quad (4.28)$$

where $\theta(x)$ is the Heaviside step function, being only non-zero (and equal to unity) for positive x . The one-dimensional solution of (4.19) is given by (4.27) with z_s taking either of the fixed values $-\lambda d$ for $|x| < d/2$ or zero otherwise. The constants of integration can be determined from the following boundary conditions

$$\delta h(-x) = \delta h(x) \quad (4.29)$$

$$\delta h(\pm x) \rightarrow 0 \quad \text{as } |x| \rightarrow \infty \quad (4.30)$$

and by imposing continuity (up to the third derivative in x) at the edges of the trench, $x = \pm d/2$. The final solution is (for positive $x \geq 0$)

$$\frac{1}{\lambda d} \delta h(x) = \begin{cases} -1 + \frac{1}{2} k_- e^{-\frac{\eta_+ d}{2}} \cosh(\eta_+ x) \\ \quad + \frac{1}{2} k_+ e^{-\frac{\eta_- d}{2}} \cosh(\eta_- x) & \text{for } 0 \leq x \leq d/2 \\ -\frac{1}{2} k_- \sinh\left(\frac{\eta_+ d}{2}\right) e^{-\eta_+ x} \\ \quad - \frac{1}{2} k_+ \sinh\left(\frac{\eta_- d}{2}\right) e^{-\eta_- x} & \text{for } x \geq d/2 \end{cases} \quad (4.31)$$

and

$$k_{\pm} = 1 \pm \frac{1}{\sqrt{1 - 4\chi^4}} \quad (4.32)$$

In Fig. 5, the membrane profile is sketched for a supported membrane (strong adhesion case) with the same parameters as those given in Table 1. The trench is specified by $d = 3a$, i.e. 148 Å, and $\lambda = 0.2$. The membrane can be seen to follow

the contour of the surface, as expected from the general prediction (4.7), without developing a similar discontinuity to that occurring at the boundary of the trench. In addition, it can be seen that an overshoot is present, with the membrane having a height greater than h_0 (for an extensive discussion of overshoots see [30]). From (4.31), $\delta h = h - h_0$ can be shown to be negative for all $x > d/2$, providing η_{\pm} are real, and so the overshoot can only arise if η_{\pm} go complex. That is, from (4.21), when $1 - 4\chi^4 < 0$ or

$$2\xi > \xi_{\sigma} \quad \text{necessary condition for overshoot} \quad (4.33)$$

i.e. in the rigidity dominated regime ($4\kappa > \sigma^2/v$).

Equation (4.33) can be understood by realizing that the rigidity term in the free energy (4.2) prevents the membrane from turning any sharp corners (see Appendix). For a pure interface ($\kappa = 0$ and $\sigma \neq 0$), (4.33) cannot be satisfied and, within our Deryagin approximation, no overshoot ever occurs.

It is also interesting to look at the extent to which the membrane penetrates into the trench. A natural measure of this quantity is the membrane height in the trench center:

$$\delta h(0) = \lambda d \left(-1 + \frac{1}{2}k_- e^{-\eta_+ d} + \frac{1}{2}k_+ e^{-\eta_- d} \right) \quad (4.34)$$

In Fig. 6 this quantity is plotted against d/a , the trench width [here, λ simply scales out – see (4.34)]. For larger d , the membrane is able to enter the trench more easily as there is less bending energy cost in the smoother configuration required to do so. For small d/a , $\delta h(0) \rightarrow 0$ and $h(0)$ tends towards the planar value of the average membrane height as the trench becomes increasingly more narrow. In the opposite limit (not yet visible in Fig. 6), $d/a \gg 1$, (4.34) implies that $\delta h(0)/a \rightarrow -\lambda d/a$, though here, we are pushing our perturbation theory beyond its region of validity.

The adhesion energy (2.12) is defined as an energy per unit of projected area. In order to obtain a finite contribution in the case of an isolated surface perturbation like a trench, we need to consider one embedded in a flat surface of *finite* lateral extent L . Hence, using a local definition, involving a cut-off L , we can write that the change in U , ΔU (up to second-order in δh) as

$$\Delta U = -\frac{1}{2L} \int_0^L dx \left\{ \sigma(\delta h')^2 + \kappa(\delta h'')^2 + v(\delta h - z_s)^2 \right\} \quad (4.35)$$

From (4.27), we can see, that for real η , the cut-off should be proportional to η_+^{-1} due to the exponential decay. However, for $\chi > 1/\sqrt{2}$ both η_+ and η_- are no longer real and it is straightforward to show that

$$\eta_+ = \eta_-^* = \frac{1}{2}\xi^{-1} \left\{ \sqrt{2\chi^2 + 1} + i\sqrt{2\chi^2 - 1} \right\} \quad (4.36)$$

where the asterisk denotes complex conjugation. In this case, (4.27) implies that for $x > d/2$ the profile has an exponential term, $\exp\left(-\frac{\sqrt{2\chi^2+1}}{2\xi}x\right)$, and so a natural

choice for L is

$$L = 8 \times \max\left(\frac{d}{2}, \frac{1}{\Re\{\eta_+\}}\right) \quad (4.37)$$

where the prefactor was chosen by examining some numerical solutions for the profile. If η_+ is complex then (4.36) implies that $1/\Re\{\eta_+\} = \frac{2\xi}{\sqrt{2\xi^2+1}}$. Using this definition $L \simeq 22.3a$ for the system specified in Table 1, which is a sensible value (see Fig. 5).

Using (4.31) and (4.35), one can show that

$$\begin{aligned} \frac{\Delta U}{\sigma} = & -\frac{\lambda^2 d}{32L} \left\{ \left(\frac{k_-}{\Lambda_+}\right)^2 I(\Lambda_+, \Lambda_+) + \left(\frac{k_+}{\Lambda_-}\right)^2 I(\Lambda_-, \Lambda_-) \right. \\ & \left. + \left(\frac{2\xi}{d}\right)^2 k_+ k_- I(\Lambda_+, \Lambda_-) \right\} \end{aligned} \quad (4.38)$$

where $\Lambda_{\pm} \equiv \eta_{\pm} d$ is introduced,

$$\begin{aligned} I(u, v) = & uv(u+v)(e^u - 1)(e^v - 1) e^{-(u+v)(\frac{1}{2} + \frac{L}{d})} \\ & \times \left[\frac{e^{(u+v)(\frac{L}{d} - \frac{1}{2})}}{1 - \frac{u(e^v - 1) + v(e^u - 1)}{ue^u(e^v - 1) + ve^v(e^u - 1)}} - \frac{1}{2} \right] \end{aligned} \quad (4.39)$$

and k_{\pm} are defined in (4.32). The function $I(u, v)$ can be seen by inspection to be positive, given that $2L \geq d$ (from (4.37)), implying that ΔU is negative. Any non-planar membrane configuration (and such a configuration must be adopted by a membrane adhering to a rough substrate) will give an additional (and dominant) bending energy cost in the definition (2.12) and so decrease U .

Equation (4.38) is illustrated in Fig. 7. The adhesion energy decreases for larger d as the membrane adopts a more and more non-planar configuration. For small d/a , one can show that (4.38) becomes

$$\frac{\Delta U}{\lambda^2 \sigma} = -\frac{a^3 \chi^4}{4\xi^2 L} \cdot \left(\frac{d}{a}\right)^3 + O\left(\left(\frac{d}{a}\right)^4\right) \quad (4.40)$$

and vanishes as $d \rightarrow 0$ in agreement with Fig. 7. For larger values of d/a , Fig. 7 would seem to imply that ΔU continues to grow in magnitude. This, of course, is false and is an unfortunate artifact of going beyond the valid limit of our perturbation theory. Exact numerical solutions for a similar scenario will be discussed in a companion paper [19] and do not exhibit such unphysical behavior.

Again, we wish to emphasize that the parameters specifying the substrate geometry (λ and d in this case) were chosen so that the constraint (4.12) was obeyed.

4.4 An isolated pit

We next consider a single cylindrical pit of radius r and depth λr . Equation (4.19) is now only a function of $\rho = \sqrt{x^2 + y^2}$ and is solved by Bessel functions, as is

usual for systems with cylindrical symmetry,

$$\delta h(\rho) = c_0 I_0(\rho\eta_-) + c_1 K_0(\rho\eta_-) + c_2 I_0(\rho\eta_+) + c_3 K_0(\rho\eta_+) + z_s \quad (4.41)$$

Here, $z_s = -\lambda r$ for $\rho < r$ and is zero elsewhere. Requiring a finite solution at $\rho = 0$ and a vanishing one as $\rho \rightarrow \infty$, implies that

$$\delta h(\rho) = \begin{cases} c_0 I_0(\rho\eta_-) + c_2 I_0(\rho\eta_+) - \lambda r & \text{for } \rho < r \\ c_1 K_0(\rho\eta_-) + c_3 K_0(\rho\eta_+) & \text{for } \rho > r \end{cases} \quad (4.42)$$

The constants of integration can be found by imposing continuity at $\rho = r$.

The cylindrical symmetry results in little qualitative changes from the previous section (see Fig. 8). Though, our perturbation theory is now acceptable up to a large hole of radius $r = 350a \simeq 0.997 \mu\text{m}$ due to the much smaller non-planar area of the substrate. A quick glance at Table 1 shows that in this case η_{\pm} are real and from (4.21) and (4.33) no overshoot can then occur [38]. This can also be seen in Fig. 8. A local adhesion energy can be defined similarly to (4.35) with the cut-off L obeying

$$L = 8 \times \max\left(r, \frac{1}{\Re\{\eta_+\}}\right) \quad (4.43)$$

Unfortunately, for this case ΔU is a very complicated expression and it is not possible to proceed analytically. Therefore, similar to Sec. 4.3, ΔU is calculated, via (4.35), with the solution (4.42) but then the integrals are evaluated numerically. One finds that U decreases with r in a similar manner to Fig. 7.

4.5 Periodic array of trenches

The next, more complicated, scenario to consider is a periodic array of one-dimensional trenches. These are of depth λd and width d in the x direction, and infinitely long in the y direction. We let the length of the repeating unit making up the surface be μd (see Fig. 9), then

$$z_s(\rho) = \frac{1}{2}\lambda d - \lambda d \sum_{n=-\infty}^{\infty} [\theta(x - n\mu d + d/2) - \theta(x - n\mu d - d/2)] \quad (4.44)$$

summing over integer n .

By ensuring that the solution is locally symmetric about each trench center, it is possible to write out, using (4.27), δh explicitly over one period

- for $0 < x < d/2$

$$\delta h(x) = c_0 \cosh(\eta_+ x) + c_1 \cosh(\eta_- x) - \frac{\lambda d}{2} \quad (4.45)$$

- for $d/2 < x < \mu d - d/2$

$$\delta h(x) = c_2 e^{\eta_+ x} + c_3 e^{-\eta_+ x} + c_4 e^{\eta_- x} + c_5 e^{-\eta_- x} + \frac{\lambda d}{2} \quad (4.46)$$

- for $\mu d - d/2 < x < \mu d$

$$\delta h(x) = c_0 \cosh(\eta_+(x - \mu d)) + c_1 \cosh(\eta_-(x - \mu d)) - \frac{\lambda d}{2} \quad (4.47)$$

As the configuration taken up by the membrane is symmetric around $x = \mu d/2$,

$$\delta h(x) = \delta h(\mu d - x) \quad (4.48)$$

one can show that

$$\begin{aligned} c_3 &= c_2 e^{\eta_+ \mu d} \\ c_5 &= c_4 e^{\eta_- \mu d} \end{aligned} \quad (4.49)$$

and so reduce the number of unknowns to four. These can be found by imposing continuity of δh and its derivatives at $x = d/2$.

The change in adhesion energy (to second-order in δh) is

$$\begin{aligned} \Delta U &= -\frac{1}{\mu d} \int_0^{d/2} dx \left[\sigma (\delta h')^2 + \kappa (\delta h'')^2 + v (\delta h + \lambda d/2)^2 \right] \\ &\quad - \frac{1}{\mu d} \int_{d/2}^{\mu d/2} dx \left[\sigma (\delta h')^2 + \kappa (\delta h'')^2 + v (\delta h - \lambda d/2)^2 \right] \end{aligned} \quad (4.50)$$

and after some algebra, can be found to satisfy

$$\frac{\Delta U}{\sigma} = -\frac{\lambda^2}{2\mu} \left[I(\Lambda_+, \Lambda_-) + I(\Lambda_-, \Lambda_+) \right] \quad (4.51)$$

where we define

$$I(u, v) = \frac{(e^u - 1)(e^{(\mu-1)u} - 1)}{e^{\mu u} - 1} \cdot \frac{uv^2}{(u^2 - v^2)^2} \left[v^2 - 2 \left(\frac{d}{\xi} \right)^2 \chi^4 \right] \quad (4.52)$$

recalling that $\Lambda_{\pm} = \eta_{\pm} d$. Again, it is possible to show that ΔU is always negative. Note, that the dependence of the adhesion energy on the depth of the trenches, via λ , is, from (4.51), simply parabolic (providing (4.12) holds).

For a surface roughness of this form, an interesting consequence of (4.51) is that the excess adhesion energy, ΔU , has a minimum as a function of μ at $\mu = \mu^*$. This is illustrated for a strongly adhering membrane in Fig. 10. If we use $\epsilon \equiv d/\xi$ as an expansion parameter, (for Fig. 10, $\epsilon \simeq 0.11$), then perturbation theory gives

$$\frac{\Delta U}{\lambda^2 \sigma} = -\frac{\mu - 1}{2\mu^2} \chi^4 \epsilon^2 + \frac{(\mu - 1)^2}{1440\mu} \cdot (\mu^2 + 2\mu - 2) \chi^8 \epsilon^6 + O(\epsilon^8) \quad (4.53)$$

which implies

$$\mu^* = 2 - \frac{\chi^4}{30} \epsilon^4 + O(\epsilon^6) \quad (4.54)$$

This can be understood by looking at the average height of the surface,

$$\begin{aligned}\langle z_s \rangle &= \frac{1}{\mu d} \int_0^{\mu d} dx z_s(x) \\ &= \frac{\lambda d}{2} \left(1 - \frac{2}{\mu}\right)\end{aligned}\quad (4.55)$$

For $1 < \mu < 2$, as μ increases, (4.55) evaluated near $\mu = 1$, implies that the surface can be visualized as an array of spikes perturbing an “initial” planar state with $\langle z_s \rangle = -\lambda d/2$. For $\mu = 1$ the substrate is flat and consequently the general solution, (4.27), implies that the membrane is so also, with $\delta h = -\lambda d/2$ and $U = U_0$. As the thickness of the spikes increases, the membrane responds and is forced to bend more and more. This costs energy and ΔU increases in magnitude. One can show that

$$\frac{\Delta U}{\sigma} = -\frac{1}{2} \left(\frac{\lambda d \chi^2}{\xi} \right)^2 (\mu - 1) + O((\mu - 1)^2) \quad (4.56)$$

for $\mu \simeq 1$. However, for $\mu > 2$, the surface (and hence the membrane) starts to tend towards another, “final”, planar state, that of $\langle z_s \rangle = \lambda d/2$ which occurs when $\mu = \infty$. As δh of the membrane, at this extreme point, also satisfies $\delta h = \lambda d/2$, $|\Delta U|$ decreases with growing μ . Looking at the two extreme values, $\mu = 1$ and $\mu = \infty$, one can see, from (4.51) and (4.52), that ΔU vanishes as expected.

This behavior becomes more transparent if the variance in the height of the surface is considered

$$\begin{aligned}\langle \Delta z_s^2 \rangle &= \langle (z_s - \langle z_s \rangle)^2 \rangle \\ &= \left(\frac{\lambda d}{\mu} \right)^2 \cdot (\mu - 1)\end{aligned}\quad (4.57)$$

with the average defined in (4.55). Equation (4.57) vanishes for $\mu = 1$ and $\mu = \infty$, and has a maximum at $\mu = 2$. Therefore, we find that the excess adhesion energy is greatest (in magnitude) for that value of μ at which the surface is the most rough, i.e. $\mu = 2$. In fact, if U is plotted against $\langle \Delta z_s^2 \rangle$, it is just a monotonically decreasing function. From (4.53) and (4.57), we have

$$\frac{\Delta U}{\sigma} = -\frac{\chi^4 \langle \Delta z_s^2 \rangle}{2d^2} \epsilon^2 + O(\epsilon^6) \quad (4.58)$$

and, at this level of approximation, there is a simple, linear relationship. The average height of the membrane itself can also be calculated

$$\begin{aligned}\langle h \rangle &= h_0 + \langle \delta h \rangle \\ &= h_0 + \frac{\lambda d}{2} \left(1 - \frac{2}{\mu}\right)\end{aligned}\quad (4.59)$$

and $\mu = 2$ again arises as a significant value.

It is also interesting to examine the extent to which the membrane penetrates each of the trenches. Concentrating on $\delta h(0)$, we find

$$\frac{\delta h(0)}{\lambda d} = \Lambda_+^2 \Lambda_-^2 \left\{ \frac{I(\Lambda_+) - I(\Lambda_-)}{\Lambda_+^2 - \Lambda_-^2} \right\} - \frac{1}{2} \quad (4.60)$$

where

$$I(u) = -\frac{e^{-u/2}}{u^2} \cdot \frac{e^{\mu u} - e^u}{e^{\mu u} - 1} \quad (4.61)$$

and $\Lambda_{\pm} = \eta_{\pm} d$. Hence, at the level of the Deryagin approximation, there is a linear dependence on the trench depth, λd . Looking at $h_0 + \delta h(0) - \langle z_s \rangle$, from (4.55), one can see (as $I(u)$ is a monotonically increasing function) that the membrane always penetrates further into the trenches as their depth grows. It experiences a more attractive potential due to the greater surface area of the substrate. However, one must be aware that increasing λ can quickly cause (4.12) to be broken.

Finally, in Fig. 11 we plot $\delta h(0)$ against the periodicity parameter, μ . It is, perhaps, at first sight surprising to see that for large μ , $\delta h(0)$ does not vanish. However, this is the wrong function with which to take this limit, as one always has at least one trench in the system and is always looking at the depth in this trench. If instead $\delta h(\mu d/2)$ is considered, this tends quite rapidly to $\lambda d/2$. For example, with the parameters given in Table 1 and Fig. 11, $\delta h(d) \simeq 0.120a$ when $\mu = 25$. Hence, the membrane returns to its height above a planar substrate. However, one can see from Fig. 11 that for $\mu \simeq 8$, the trenches no longer have a significant effect and $\delta h(0)$ plateaus; the membrane effectively experiences a potential generated by a flat surface.

4.6 Self-affine surfaces

In this penultimate section, we describe surfaces whose roughness is random in character. This is normally used to model the ‘‘natural’’ roughness of a substrate which arises due to chemical impurities or crystal defects. We adopt the self-affine approximation [39] and assume that the substrate appears relatively smooth on large lengthscales. Typical fluctuations of length L grow only as L^{β} where β is the roughness exponent $0 \leq \beta \leq 1$, which is directly analogous to the thermal roughness of an interface [23]. However, such models become divergent as $L \rightarrow \infty$ and we prefer to adopt a reduced self-affine scaling law [40] where a long lengthscale cut-off has been explicitly included

$$\langle |z_s(\boldsymbol{\rho}' + \boldsymbol{\rho}) - z_s(\boldsymbol{\rho}')|^2 \rangle = 2\gamma^2 \left(1 - e^{-\left(\frac{\ell}{\zeta}\right)^{2\beta}} \right) \quad (4.62)$$

or equivalently

$$\langle z_s(\mathbf{0}) z_s(\boldsymbol{\rho}) \rangle = \gamma^2 e^{-\left(\frac{\ell}{\zeta}\right)^{2\beta}} \quad (4.63)$$

Here γ is the saturated root mean square roughness at long lengthscales, and ζ is the crossover length from self-affine to saturated behavior. The wetting properties of such surfaces ($\kappa = 0$) have already been quite extensively studied [13, 18].

To be able to calculate the membrane adhesion energy analytically, we specialize to two cases:

4.6.1 Roughness $\beta = 1$

Equation (4.63) can be Fourier transformed to give

$$\langle \tilde{z}_s(\mathbf{p}) \tilde{z}_s(\mathbf{q}) \rangle = 4\pi^3 \gamma^2 \zeta^2 e^{-\frac{\zeta^2 q^2}{4}} \delta(\mathbf{p} + \mathbf{q}) \quad (4.64)$$

which can then be used in (4.11) to calculate ΔU . We find that

$$\frac{\Delta U}{\sigma} = -\frac{1}{8} \left(\frac{\gamma \mathcal{X}^2}{\xi} \right)^2 \left\{ 4 + \left(\frac{\zeta \mathcal{X}}{\xi} \right)^4 \left[\frac{I(\Lambda_+) - I(\Lambda_-)}{\Lambda_+^2 - \Lambda_-^2} \right] \right\} \quad (4.65)$$

where

$$I(u) = e^{\frac{u^2}{4}} \Gamma \left(0, \frac{u^2}{4} \right) \quad (4.66)$$

$$\Lambda_{\pm} = \zeta \eta_{\pm} \quad (4.67)$$

and

$$\Gamma(0, u) = \int_u^{\infty} dz \frac{e^{-z}}{z} \quad (4.68)$$

is an incomplete Gamma function.

4.6.2 Roughness $\beta = \frac{1}{2}$

In this case we have

$$\langle \tilde{z}_s(\mathbf{p}) \tilde{z}_s(\mathbf{q}) \rangle = \frac{2\pi^3 \gamma^2 \zeta^2}{(1 + \zeta^2 q^2)^{\frac{3}{2}}} \delta(\mathbf{p} + \mathbf{q}) \quad (4.69)$$

and

$$\frac{\Delta U}{\sigma} = -\frac{1}{8} \left(\frac{\gamma \mathcal{X}^2}{\xi} \right)^2 \left\{ 1 + \left(\frac{\zeta \mathcal{X}}{\xi} \right)^4 \left[\frac{I(\Theta_+) - I(\Theta_-)}{\Theta_+^2 - \Theta_-^2} \right] \right\} \quad (4.70)$$

with

$$I(u) = \frac{1}{u^2} + \frac{1}{2u^3} \log \left(\frac{1-u}{1+u} \right) \quad (4.71)$$

and

$$\Theta_{\pm}^2 = 1 - (\zeta \eta_{\pm})^2 \quad (4.72)$$

For $\gamma = 4a$, equations (4.65) and (4.70) are illustrated in Fig. 12. As the crossover length, ζ , grows, the disorder becomes more and more correlated and the substrate becomes smoother on larger lengthscales. One can see that in both cases, U is tending towards the planar value. For smaller β , this plateau is reached more quickly in accordance with (4.63). As ζ decreases and the substrate becomes rougher, the adhesion energy deviates further and further away from the planar value.

4.7 Tensionless membranes

So far we have only considered membranes which have a finite tension, σ , and now, for the sake of completeness, we will briefly illustrate how our results change in the limit of $\sigma \rightarrow 0$. For vanishing membrane tension, the definitions (2.16, 4.21) and (4.22) imply that

$$\eta_{\pm} = \pm \frac{1}{\sqrt{2}}(1 \pm i)\xi_{\kappa}^{-1} \quad \text{for } \sigma = 0 \quad (4.73)$$

Equation (4.27) then indicates that the profile will have an oscillatory though exponentially damped form.

To see how the adhesion energy changes, we can look at, for example, the adhesion energy of Sec. 4.5, equation (4.51) which is valid for a surface periodically patterned with trenches. Multiplying (4.51) by σ , one is naturally led to consider

$$\frac{\sigma \chi^4}{\xi^2} \rightarrow \kappa \xi_{\kappa}^{-4} \quad (4.74)$$

in the limit of zero tension. A little thought then gives

$$\Delta U = \frac{\lambda^2}{\mu} \left(\frac{d}{\xi_{\kappa}} \right)^2 \kappa \xi_{\kappa}^{-2} \left[I(\Lambda_+, \Lambda_-) + I(\Lambda_-, \Lambda_+) \right] \quad (4.75)$$

with

$$I(u, v) = \frac{(e^u - 1)(e^{(\mu-1)u} - 1)}{e^{\mu u} - 1} \cdot \frac{uv^2}{(u^2 - v^2)^2} \quad (4.76)$$

and $\Lambda_{\pm} = d\eta_{\pm}$, with the η 's obeying (4.73). While it is not as obvious as before, ΔU is again negative.

5 Discussion

In this paper, we have looked at the effect of geometric surface structure on the adhesion properties of a membrane and a solid substrate. The membrane interacts with the substrate via a Van der Waals potential and experiences either a Helfrich-like entropic repulsion, if it is weakly adhering, or hydration forces, if it is strongly adhering or supported. We find that the most analytically successful approach is that of Deryagin in which the entire interaction potential is assumed to be a local function of height. By making a further harmonic approximation quite a large number of surface geometries can be solved for. In general, the membrane tries to follow the surface contour of the substrate but for short wavelength undulations is damped due to its tension and rigidity. Two lengthscales, ξ_{σ} and ξ_{κ} , analogous to the ‘‘healing’’ length [16] for interfaces, emerge and control this damping.

Within the Deryagin description, we find that the membrane can overshoot (similar to the behavior in a laser trap [29]) near a disturbance in the planar

structure of the surface. Overshooting (i.e having a height greater than that it would have had for a completely flat surface) is seen to be a consequence of the eigenvalues of the 4th order operator, making up the Euler-Lagrange equation, going complex. This occurs for $2\xi > \xi_\sigma$ and consequently is directly due to the membrane having a finite (non-zero) rigidity.

In general (but still at the Deryagin level), increasing the roughness of the surface reduces the membrane adhesion’s energy. Having a non-planar substrate immediately leads to a competition between the bending and potential energy contributions to the free energy; the bending energy tries to flatten the membrane and so move it away from the surface to heights where the effect of the geometrical heterogeneity is washed out. On the other hand, the potential energy, which, due to the larger surface area of the substrate, is more attractive than in the planar case, acts to bring the membrane in closer. As the elastic or bending energy of a membrane contains a rigidity term it always dominates over the potential energy (for a membrane exhibiting a sharp kink configuration this rigidity contribution even diverges – see Appendix) and thus the adhesion energy is reduced. For a flat substrate, the bending energy contribution is zero and this rivalry does not exist.

This inverse dependence of U on the roughness of the substrate is perhaps best illustrated in Fig. 10, where by changing μ we move through different surface configurations whose roughness function (the variance of z_s) passes through a minimum. The adhesion energy can be clearly seen to mimic such behavior. In Fig. 4, the importance of the bending energy is again shown; with U decreasing as the rigidity, κ , increases.

Figures 6 and 11 describe the extent to which the membrane penetrates into an indentation in the substrate surface. Generally, the membrane extends more extensively into a wider trench; the bending energy of the resulting configuration is less — the membrane is flatter, and the potential energy gain is also greater as the membrane is more able to straighten out at the trench base.

As mentioned in the introduction, supported membranes are invaluable for the construction of biosensors. The proteins that endow the membrane with this properties can, unfortunately, disturb it from a favorable planar configuration. One way to surmount this problem is to indent the substrate with pockets which then act as “docking” pods for the proteins. However, this technique can backfire if the membrane itself changes its configuration significantly in response to the now non-planar surface. Our theoretical work predicts that the narrower the trench or pocket, Fig. 6, and the more widely spaced apart they are, Fig. 11, the less likely such an event occurs. We also find that, within the Deryagin framework, increasing the depth of the trenches encourages the membrane to penetrate further into them.

Finally, we looked at randomly rough or self-affine surfaces where the general principles outlined above still hold. Rougher surfaces (those with a larger β exponent) have smaller adhesion energies, see Fig. 12.

In an accompanying paper [19], we will explore non-local methods, which enable progress beyond the Deryagin approximation, and also will perform some

exact numerical calculations. We intend to extend the method to include chemical heterogeneity. This then opens up the possibility of modeling chemically *and* geometrically structured substrates which are becoming crucial to recent pioneering biotechnological research.

Acknowledgments

We are particularly grateful to J. Rädler and E. Sackmann for introducing us to the problem of membrane adhesion on rough surfaces, for numerous discussions and suggestions, and for sharing with us their experimental results. We greatly benefited from conversations and correspondence with M. Kozlov, A. Marmur, P. Lenz, R. R. Netz, M. O. Robbins, U. Seifert and P. B. Sunil Kumar. PSS would like to thank the British Council, the Israeli Ministry of Science and the Sackler Institute for Theoretical Physics (Tel Aviv University) for providing financial support during a visit to Israel, where the majority of this work was carried out. Partial support from the Israel Science Foundation founded by the Israel Academy of Sciences and Humanities — centers of Excellence Program and the U.S.-Israel Binational Foundation (B.S.F.) under grant No. 94-00291 is gratefully acknowledged.

Appendix: Kink configurations in membranes and interfaces

In this appendix, we consider the elastic energy cost of a membrane adopting a configuration containing sharp kinks. Let us, for the purpose of illustration, consider a one-dimensional membrane embedded in a two-dimensional space having the profile

$$h(x) = c \tanh\left(\frac{x}{\epsilon L}\right) \quad (5.1)$$

with the two lengths L and c obeying $L \gg c$. In the limit of $\epsilon \rightarrow 0$, $h(x)$ develops two sharp kinks

$$\lim_{\epsilon \rightarrow 0} h(x) = c[2\theta(x) - 1] \quad (5.2)$$

and becomes a step function. We can examine the effect this has on the asymptotic behaviors of the two adhesion energy densities (per unit area)

$$u_\sigma = \frac{\sigma}{2L} \int_{-L}^L dx \sqrt{1 + h'^2} \quad (5.3)$$

and

$$u_\kappa = \frac{\kappa}{2L} \int_{-L}^L dx \frac{h''^2}{(1 + h'^2)^{\frac{5}{2}}} \quad (5.4)$$

Equations (5.3) and (5.4) provide the contributions to the free energy from the tension (interface-like) and the rigidity (membrane-like) terms in (2.2), respectively.

The interfacial elastic energy cost is simply proportional to the length of the membrane in the step configuration

$$\begin{aligned} u_\sigma &\simeq \frac{\sigma}{2L} \cdot 2(L+c) \\ &\sim \sigma \end{aligned} \tag{5.5}$$

where we have taken the limit of $\epsilon \rightarrow 0$. This is clearly finite.

To find the asymptotic limit of the rigidity contribution, we notice that

$$u_\kappa = \frac{2c^2\epsilon\kappa}{L^5} \int_{-L}^L dx \frac{\tanh^2\left(\frac{x}{\epsilon L}\right) \cosh^{-4}\left(\frac{x}{\epsilon L}\right)}{\left[\epsilon^2 + \left(\frac{c}{L}\right)^2 \cosh^{-4}\left(\frac{x}{\epsilon L}\right)\right]^{\frac{5}{2}}} \tag{5.6}$$

is an even function and so, writing $t = \tanh\left(\frac{x}{\epsilon L}\right)$, we have

$$u_\kappa = \frac{4c^2\kappa}{\epsilon^3 L^4} \int_0^{\tanh(1/\epsilon)} dt \frac{t^2(1-t^2)}{\left[1 + \left(\frac{c}{\epsilon L}\right)^2 (1-t^2)^2\right]^{\frac{5}{2}}} \tag{5.7}$$

which can be integrated by parts

$$u_\kappa \sim \frac{2\kappa}{3L^2\epsilon} \left\{ 1 - \int_0^{\tanh(1/\epsilon)} \frac{dt}{\left[1 + \left(\frac{c}{L} \left(\frac{1-t^2}{\epsilon}\right)\right)^2\right]^{\frac{3}{2}}} \right\} \tag{5.8}$$

As

$$\lim_{\epsilon \rightarrow 0} \left\{ \frac{1 - \tanh^2(1/\epsilon)}{\epsilon} \right\} = 0 \tag{5.9}$$

the integral in (5.8) is well-defined and finite.

Therefore, for small ϵ , we have

$$u_\sigma \sim \sigma \quad \text{and} \quad u_\kappa \sim \frac{\kappa}{L^2} \epsilon^{-1} \tag{5.10}$$

and so the tension or interface-like contribution is constant while that from the rigidity (membrane-like) diverges – an interface ($\kappa = 0$ and $\sigma \neq 0$) can have a configuration with a sharp kink while a membrane cannot.

References

- [1] See, for example, *Structure and Dynamics of Membranes*; Lipowsky R. and Sackmann E., Eds.; Elsevier: Amsterdam, 1995.
- [2] Alberts B., Bray D., Johnson A., Lewis J., Raff M., Roberts K. and Walter P. *Essential Cell Biology*; Garland Publishing: New York, 1998.
- [3] Lasic D. D. In *Structure and Dynamics of Membranes*; Lipowsky R. and Sackmann E., Eds.; Elsevier: Amsterdam, 1995; p 491–519.
- [4] Seifert U. and Lipowsky R. Phys. Rev. A **1990**, *42*, 4768. Kraus M., Seifert U. and Lipowsky R. Europhys. Lett. **1995**, *32*, 431.
- [5] Seifert U. Phys. Rev. Lett. **1995**, *74*, 5060.
- [6] Rädler J. O., Feder T. J., Strey H. H. and Sackmann E. Phys. Rev. E **1994**, *51*, 4526.
- [7] Sackmann E. Science **1996**, *271*, 43. Rädler J. and Sackmann E. Curr. Opin. Solid State Material Sci. **1997**, *2*, 330.
- [8] Salafsky J., Groves J. T. and Boxer S. G. Biochemistry **1996**, *35*, 14773.
- [9] Gerdes S. and Ström G. Colloids Surfaces A **1996**, *116*, 135.
- [10] Spatz J. P., Herzog T., Mössmer S., Ziemann P. and Möller M. Adv. Mater. **1999**, *11*, 149.
- [11] Wolansky G. and Marmur A. Langmuir **1998**, *14*, 5292.
- [12] Swain P. S. and Lipowsky R. Langmuir **1998**, *14*, 6772.
- [13] Kardar M. and Indekeu J. O. Europhys. Lett. **1990**, *12*, 161. Li H. and Kardar M. Phys. Rev. B **1990**, *42*, 6546. Sartoni G., Stella A. L., Giugliarelli G. and Dorsogna M. R. Europhys. Lett. **1997**, *39*, 633.
- [14] Parry A. O., Swain P. S. and Fox J. A. J. Phys.: Condens. Matter **1996**, *8*, L659. Swain P. S. and Parry A. O. Eur. Phys. J. B **1998**, *4*, 459.
- [15] Gau H., Herminghaus S., Lenz P. and Lipowsky R. Science **1999**, *283*, 46.
- [16] Andelman D., Joanny J. F. and Robbins M. O. Europhys. Lett. **1988**, *7*, 731. Robbins M. O., Andelman D. and Joanny J. F. Phys. Rev. A **1991**, *43*, 4344.
- [17] Netz R. R. and Andelman D. Phys. Rev. E **1997**, *55*, 687.
- [18] Harden J. L. and Andelman D. Langmuir **1992**, *8*, 2547.
- [19] Swain P. S. and Andelman D., to be published.

- [20] Canham P. B. J. *Theoret. Biol.* **1970**, *26*, 61. Helfrich W. Z. *Naturforsch. C* **1973**, *28*, 693.
- [21] Lipowsky R. In *Structure and Dynamics of Membranes*; Lipowsky R. and Sackmann E., Eds.; Elsevier: Amsterdam, 1995; p 521–602.
- [22] Israelachvili J. N. *Intermolecular and Surface Forces*; Academic Press: London, 1992.
- [23] Lipowsky R. and Fisher M. E. *Phys. Rev. B* **1987**, *36*, 2126.
- [24] Helfrich W. Z. *Naturforsch.* **1978**, *33*, 305.
- [25] Helfrich W. and Servuss R. M. *Il Nuovo Cimento D* **1984**, *3*, 137.
- [26] Evans E., *Langmuir* **1991**, *7*, 1900.
- [27] Netz R. R. and Lipowsky R. *Europhys. Lett.* **1995**, *29*, 345.
- [28] Bruinsma R., Goulian M. and Pincus P. *Biophys. J.* **1994**, *67*, 746.
- [29] Bar-Ziv R., Menes R., Moses E. and Safran S. A. *Phys. Rev. Lett.* **1995**, *75*, 3356.
- [30] Menes R. and Safran S. A. *Phys. Rev. E* **1997**, *56*, 1891.
- [31] Netz R. R. *J. Phys. (France) I* **1997**, *7*, 833.
- [32] Lipowsky R. and Leibler S. *Phys. Rev. Lett.* **1986**, *56*, 2541.
- [33] Gawrisch K., Ruston D., Zimmerberg J., Parsegian V. A., Rand R. P. and Fuller N. *Biophys. J.* **1992**, *61*, 1213.
- [34] de Gennes P. G. *Rev. Mod. Phys.* **1985**, *57*, 827.
- [35] Johnson S. J., Bayerl T. M., McDermott D. C., Adam G. W., Rennie A. R., Thomas R. K. and Sackmann E. *Biophys. J.* **1991**, *59*, 289.
- [36] Deryagin B. V., *Kolloidn. Zh.* **1955**, *17*, 827. Deryagin B. V., Churaev N. V. and Muller V. M. *Surface Forces*; Consultants Bureau: New York, 1987.
- [37] Assuming (4.12) is still valid.
- [38] Similarly to the exponentials in (4.27), $K_0(\eta)$ and $I_0(\eta)$ are single valued functions for real $\eta > 0$ and so an overshoot can only occur for complex η .
- [39] See, for example, the review article by Forgacs G., Lipowsky R. and Nieuwenhuizen Th. M. In *Phase Transitions and Critical Phenomena*; Domb C. and Lebowitz J. L., Eds.; Academic Press: London, 1991; Vol. 14.
- [40] Sinha S. K., Sirota E. B., Garoff S. and Stanley H. B. *Phys. Rev. B* **1988**, *38*, 2297.

$\kappa = 35T$	$\sigma = 1.7 \times 10^{-5} \text{ Jm}^{-2}$	$\delta = 38 \text{ \AA}$	$p = 0$
$\Omega \simeq 8.07 \times 10^7 \text{ m}^{-1}$	$b \simeq 5.47 \times 10^4$	$\alpha^{-1} = 2.2 \text{ \AA}$	$T = 4.1 \times 10^{-21} \text{ J}$
WEAK ADHESION			
$A = 8.67 \times 10^{-22} \text{ J}$	$a \simeq 28.5 \text{ \AA}$	$h_0 \simeq 11.85a \simeq 338 \text{ \AA}$	$U_0 \simeq 1.1 \times 10^{-4} \sigma$
$\xi \simeq 32.25a$	$v \simeq 8.04 \times 10^{-6} a^{-2} \sigma$	$\xi_\sigma \simeq 352.62a$	$\xi_\kappa \simeq 106.64a$
$\chi \simeq 0.302$	$\eta_+ \simeq 0.0309a^{-1}$	$\eta_- \simeq 0.0028a^{-1}$	$L \simeq 259.1a$
STRONG ADHESION (supported membrane)			
$A = 2.6 \times 10^{-21} \text{ J}$	$a \simeq 49.3 \text{ \AA}$	$h_0 \simeq 0.61a \simeq 30 \text{ \AA}$	$U_0 \simeq 0.298\sigma$
$\xi \simeq 18.62a$	$v \simeq 22.85a^{-2} \sigma$	$\xi_\sigma \simeq 0.21a$	$\xi_\kappa \simeq 1.97a$
$\chi \simeq 9.44$	$\eta_+ \simeq (0.359 + 0.357i)a^{-1}$	$\eta_- \simeq (0.359 - 0.357i)a^{-1}$	$L \simeq 22.3a$

Table 1: The various parameters, chosen and calculated, for the planar system and for both weak and strong adhesion. For definitions see text.

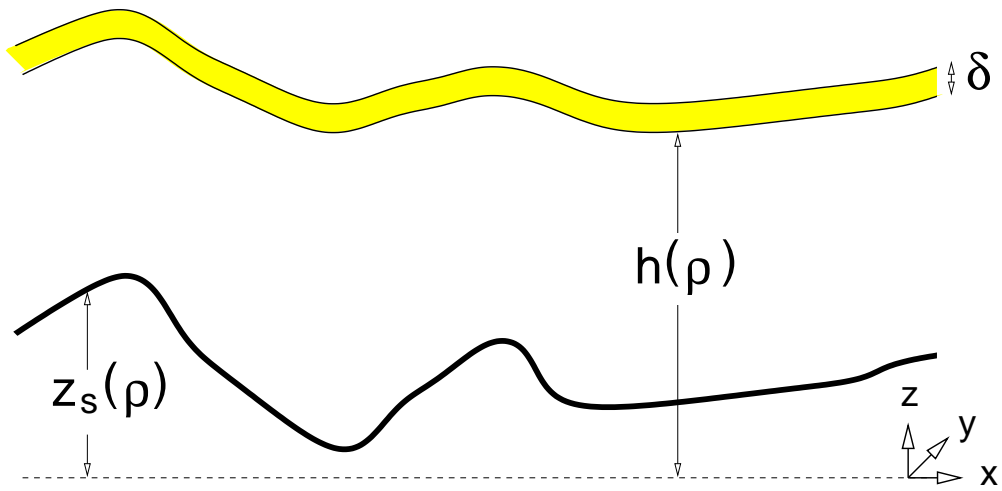


Figure 1: A membrane adhering to a rough surface. The reference ρ -plane is shown as a dashed line. The height of the lower membrane lipid leaflet and the surface, measured from this plane, are denoted by $h(\rho)$ and $z_s(\rho)$, respectively. The membrane thickness is δ .

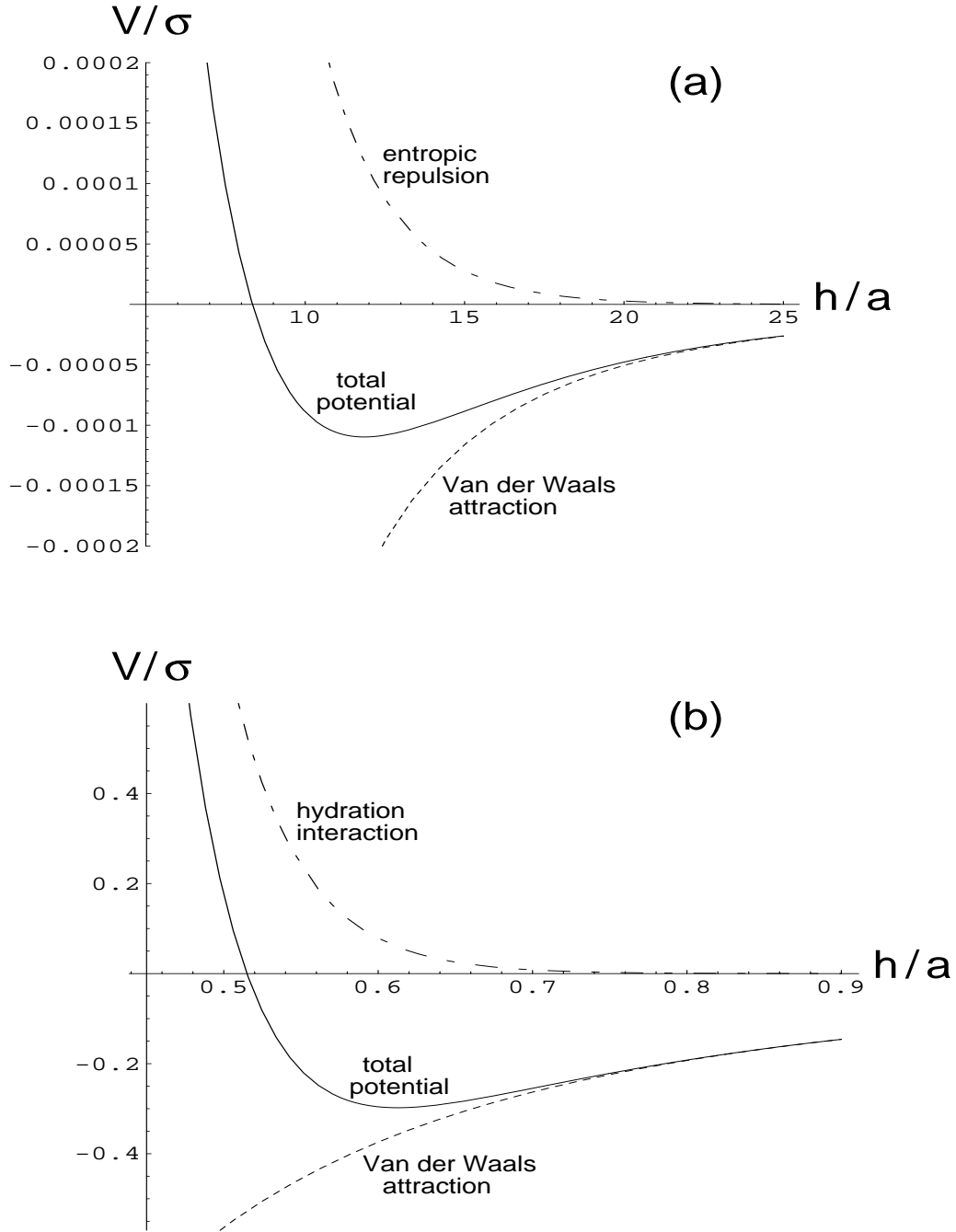


Figure 2: A plot of the various interactions described in Sec. 2, with parameter values given in Table 1, for a membrane weakly (a) and strongly (b) adhering to a planar substrate. Here all potentials are measured in units of the tension, $\sigma = 1.7 \times 10^{-5} \text{Jm}^{-2}$, and lengths in terms of a . The system can be seen to equilibrate at $h_0 \simeq 12a$ and $h_0 \simeq 0.6a$ for weak and strong adhesion, respectively.

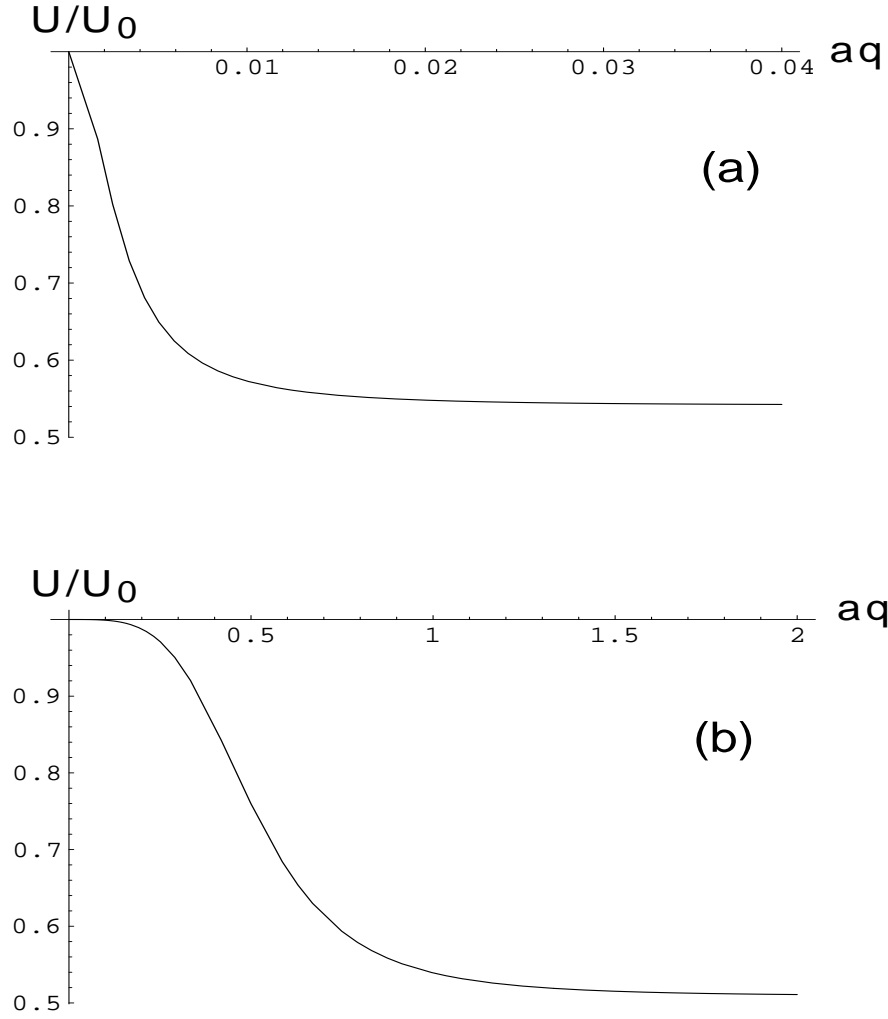


Figure 3: A plot of the adhesion energy versus the rescaled wavenumber aq of a sinusoidally corrugated surface. For weak adhesion (a), the surface amplitude is set to $c = 5a \simeq 143 \text{ \AA}$ while for a strongly adhering membrane (b) it is much smaller, $c = 0.16a \simeq 8 \text{ \AA}$. All other parameters are given in Table 1. For these values of c , U soon reaches a small (< 1) asymptotic value which implies that our perturbation theory remains valid for all q .

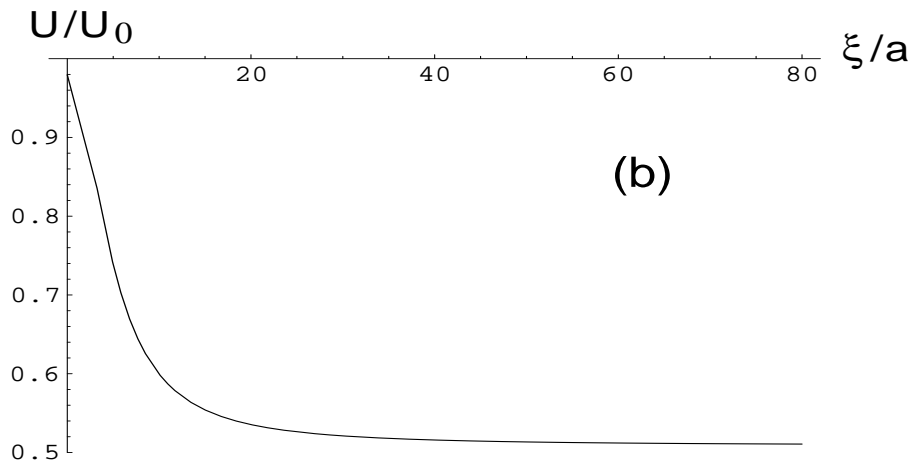
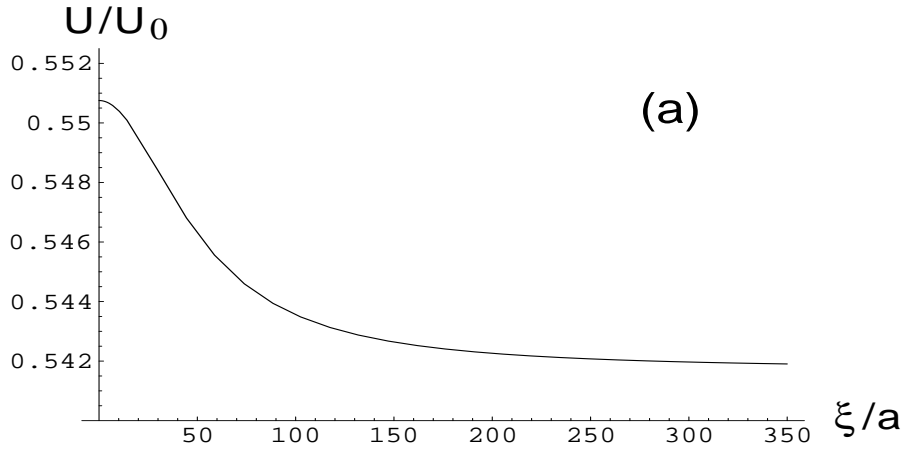


Figure 4: The adhesion energy for a weakly (a) and strongly (b) adhering membrane above a corrugated surface. This has $c = 5a \simeq 143\text{\AA}$ and $q = 0.02/a$ for the former and $c = 0.16a \simeq 8\text{\AA}$ and $q = 1/a$ for the latter. Increasing ξ/a corresponds to increasing κ/A . All other parameter values are given in Table 1.

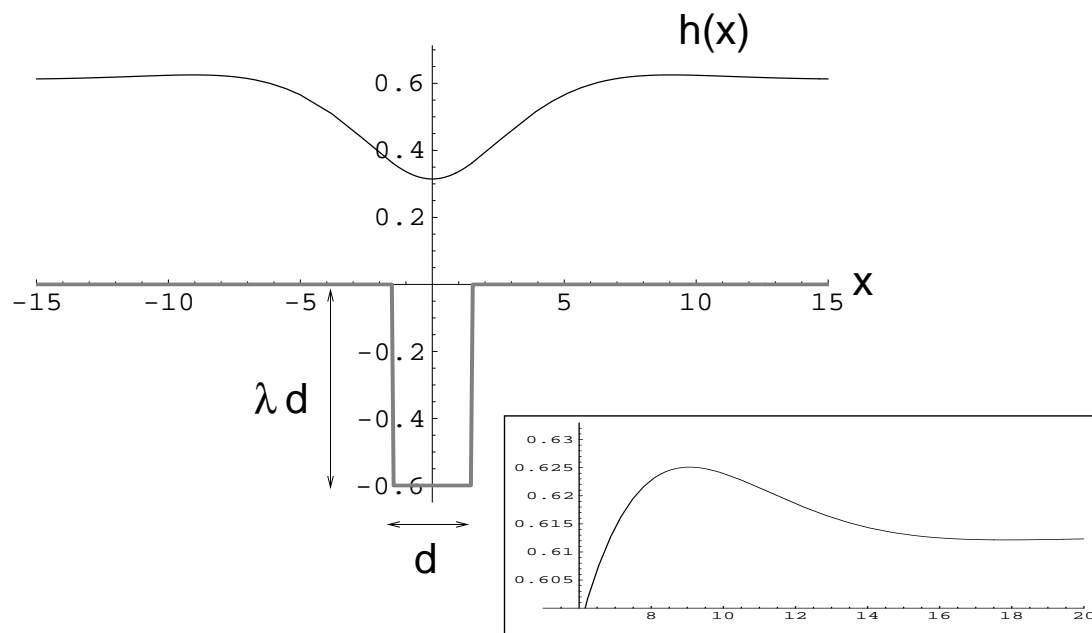


Figure 5: The membrane profile $h(x)$ for strong adhesion to a solid surface (thick line) broken by a single trench of width $d = 3a \simeq 148\text{\AA}$ and depth λd with $\lambda = 0.2$. The inset region shows a blow up of the profile with scales chosen so as to emphasize the overshoot present. The local adhesion energy $U/U_0 \simeq 0.51$. All lengths are stated in units of a without explicit statements for clarity. Parameter values are given in Table 1 (strong adhesion) and only the lower lipid leaflet is shown.

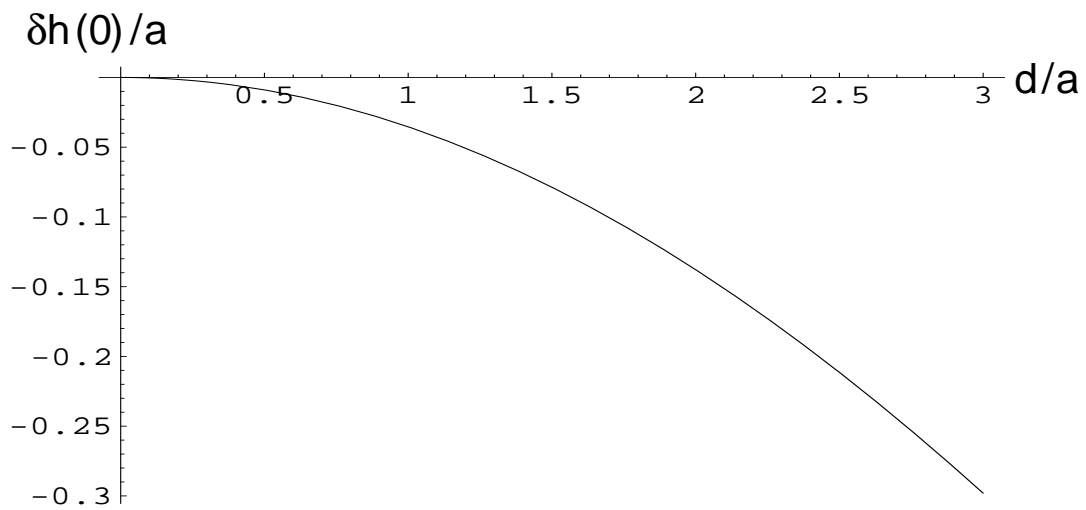


Figure 6: The height of the membrane $\delta h(0) = h(0) - h_0$ at the center of an isolated trench of width d and depth λd , where $\lambda = 0.2$. See Table 1 (strong adhesion) for choices of the other parameters.

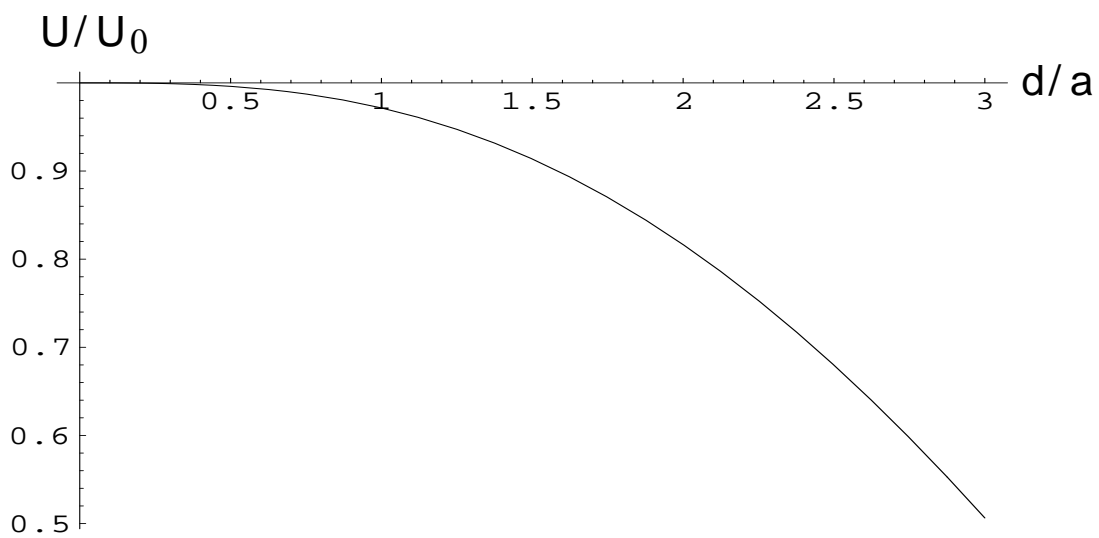


Figure 7: The relative adhesion energy, U/U_0 plotted for a trench of width d and depth λd , with $\lambda = 0.2$. For an isolated, non-planar perturbation of the substrate, a local definition of the adhesion energy needs to be used and involves the cut-off L (see text). All other parameters used here are given in Table 1 (strong adhesion case).

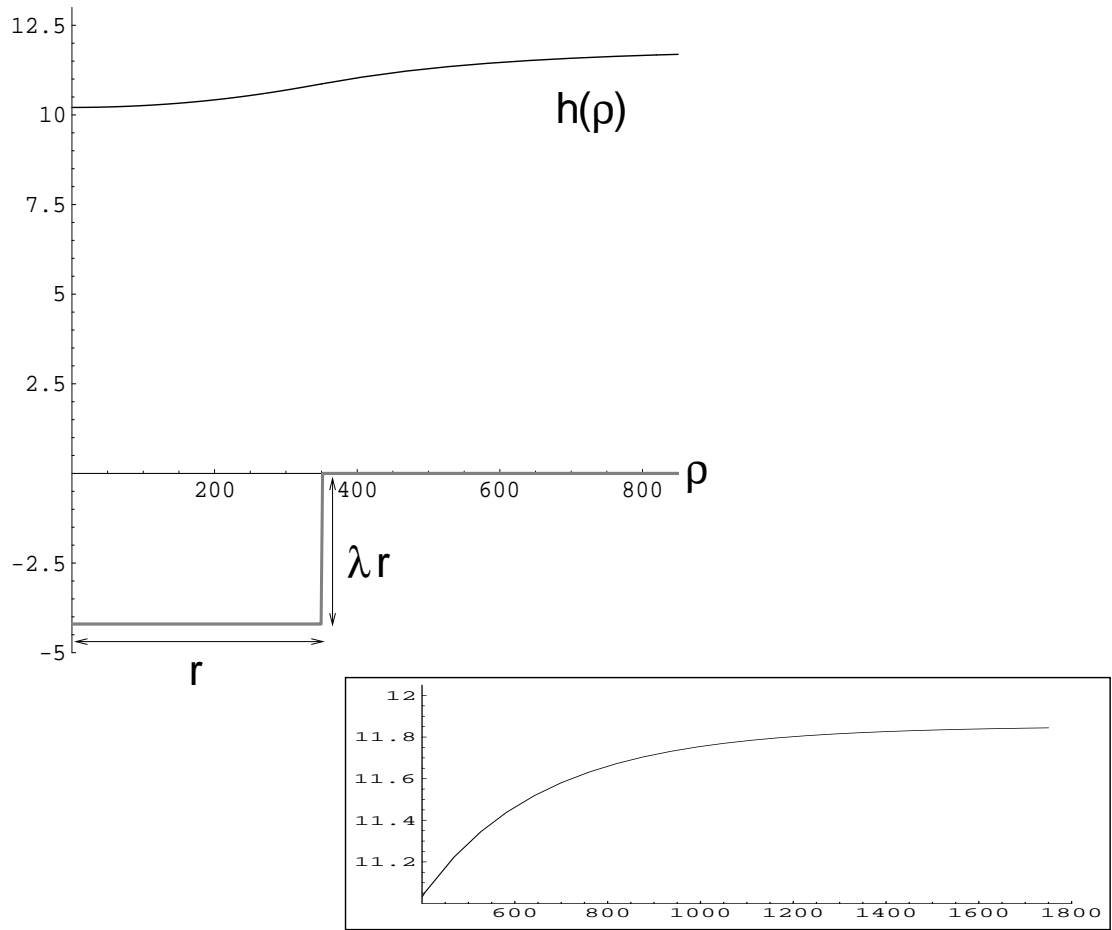


Figure 8: A typical membrane configuration $h(\rho)$ (of the lower lipid leaflet) weakly adhering over a cylindrically symmetric pit of depth λr and radius r . Here $\lambda = 0.012$ and $r = 350a \simeq 0.997 \mu\text{m}$ (for further choices see Table 1 – weak adhesion). The local adhesion energy (with $L \simeq 259.1a$) is $U/U_0 \simeq 0.50$. The inset shows that no overshoot is present as η_{\pm} are now real. All lengths are given in units of a .

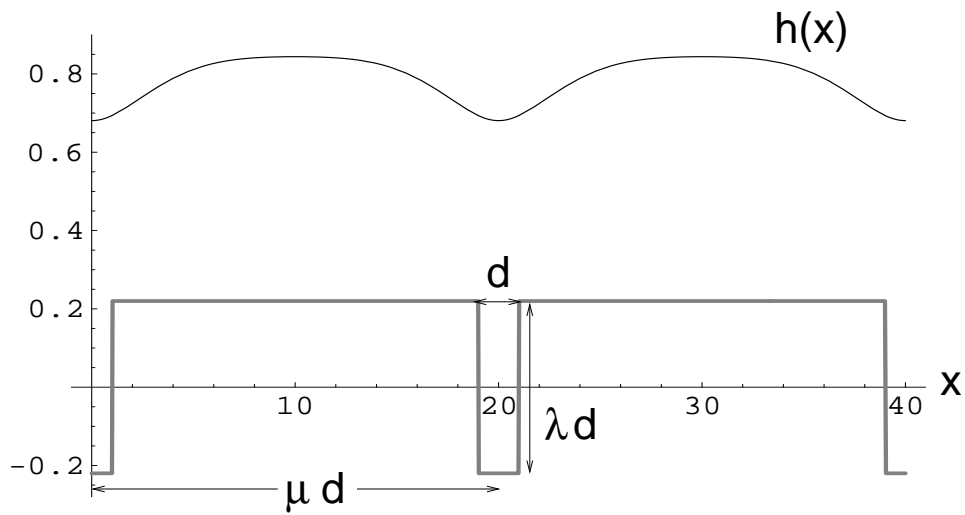


Figure 9: The profile of a membrane $h(x)$ supported (strong adhesion) above a periodically structured substrate with trenches of infinite length, width d and depth λd . We have set $\lambda = 0.22$, $\mu = 10$ and $d = 2a \simeq 99 \text{ \AA}$ in the above. The membrane configuration (thin line) follows that of the substrate (thick line) but at a much reduced amplitude (due to the effects of rigidity and tension). All lengths are shown in units of a .

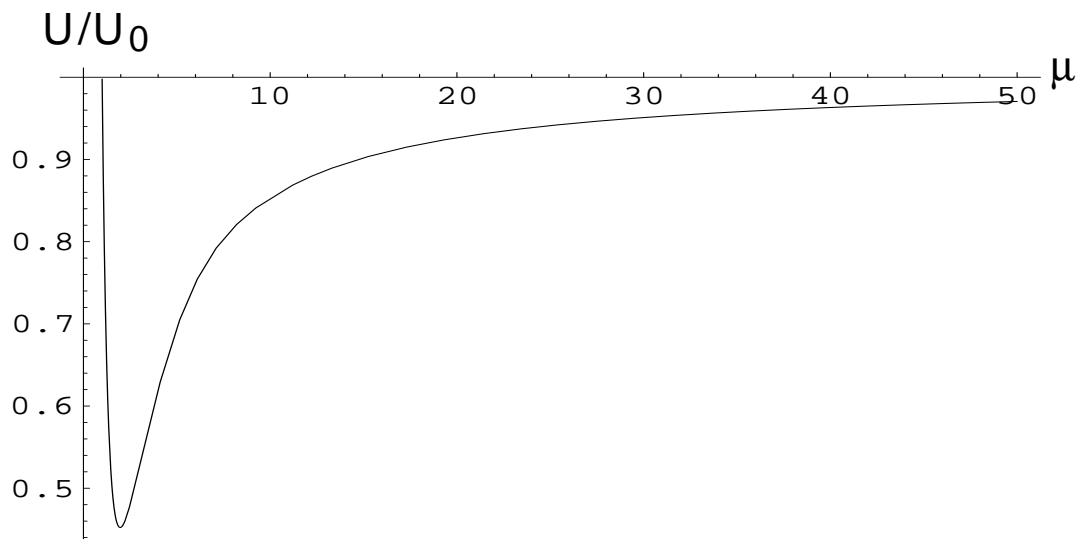


Figure 10: For $\lambda = 0.12$ and $d = 2a \simeq 99\text{\AA}$, the relative adhesion energy U/U_0 in the strong adhesion case is plotted against μ , the periodicity parameter. For the two flat limiting surfaces, $\mu = 1$ and $\mu = \infty$, the decrement ΔU is zero and $U = U_0$. The minimum in the curve occurs near $\mu = 2$ as described in Sec. 4.5.

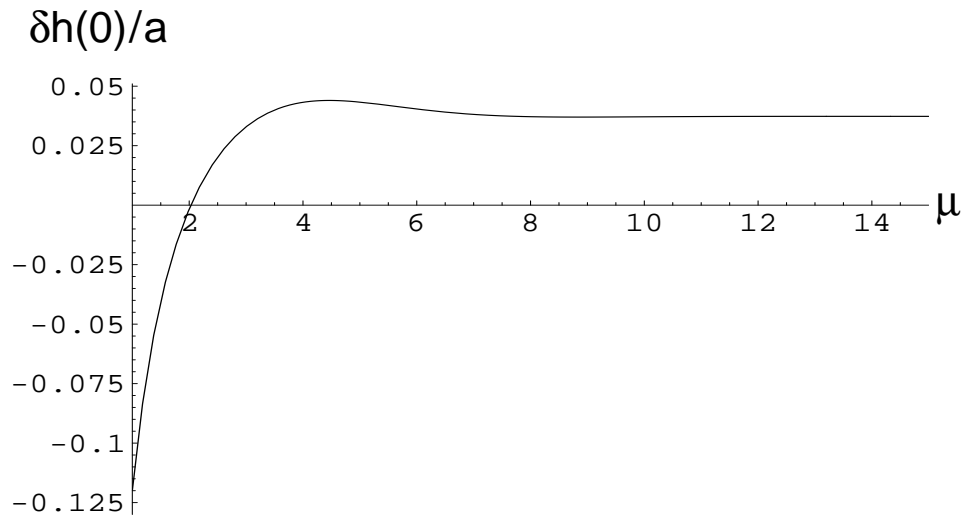


Figure 11: The height deviation of the membrane in the middle of a trench (strong adhesion), $\delta h(0) = h(0) - h_0$, as a function of μ for fixed $\lambda = 0.12$ and $d = 2a \simeq 99\text{\AA}$.

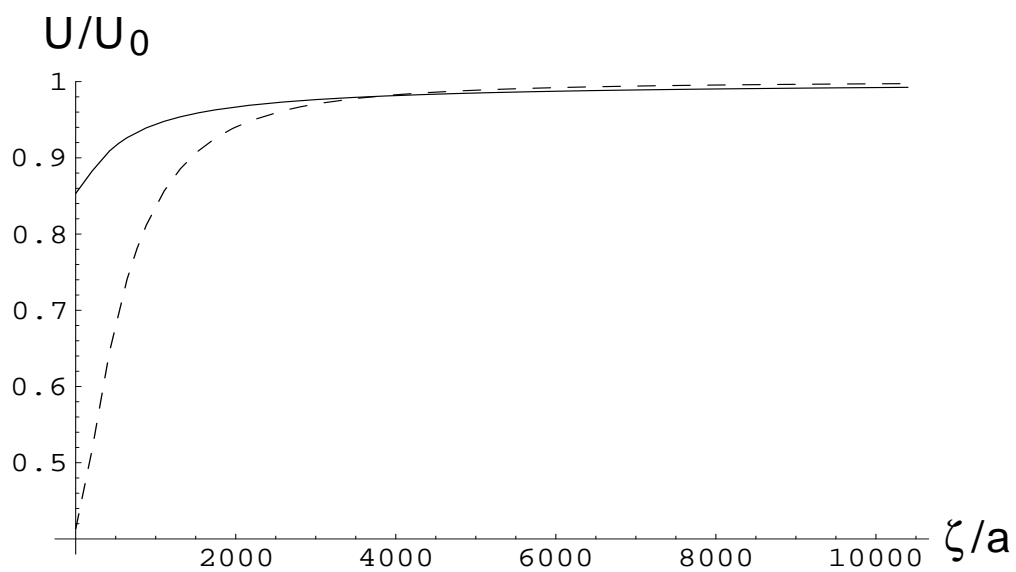


Figure 12: The relative adhesion energy for a weakly adhering membrane above two different self-affine surfaces plotted against ζ , the crossover length; the full curve is for $\beta = \frac{1}{2}$ while the dashed is $\beta = 1$. Here, $\gamma = 4a$, that is $\gamma \simeq 114 \text{ \AA}$ and all other parameter values are given in Table 1 (weak adhesion).